

**High-pressure subsolidus and melting phase relations of  
Na-rich plagioclase: implications for the shock  
metamorphism of plagioclase in shocked meteorites**

愛媛大学大学院 理工学研究科

先端科学特別コース

**Youmo Zhou (周 佑黙)**

**June 2017**

**High-pressure subsolidus and melting phase relations of  
Na-rich plagioclase: implications for the shock  
metamorphism of plagioclase in shocked meteorites**

**Youmo Zhou (周 佑默)**

Supervisors: Prof. Tetsuo Irifune (入船 徹男 教授)

Prof. Toru Inoue (井上 徹 教授)

Prof. Hiroaki Ohfuji (大藤 弘明 教授)

(Submitted to Graduate School of Science and Engineering, Ehime University,  
in Partial Fulfillment of the Requirements for the Degree of Doctor of Science)

Ehime University, Matsuyama, Ehime, Japan

June 2017

## Acknowledgement

After my short-term study in MIT (Muroran Institute of Technology, Japan), I began to love this beautiful and amazing country, and decided to learn more as a doctoral student there. As a man of high pressure, I could not miss GRC, Ehime University, where the hardest nanopolycrystalline diamond (Hime Dia) was created by the most advanced high-pressure and high-temperature techniques. So I tried my best luck, and sent out my will.

Ignoring my poor background, Prof. Irifune kindly accepted me, and provided me a strong financial support so that I enjoyed a carefree life in Japan. More importantly, he showed me a world of geoscience, and gave me freedom in research. Thanks to the 3-years training and practice, now I can feel the enhancement in knowledge and experimental skill that happened to me. Although I am still a beginner of geoscience, I feel confident to become better in the future.

Highly based on the guidance and suggestions given by my supervisors and other GRC members, I made something cool during the 3 years, including an easy way of generating high temperatures up to 3000 K under high pressures of 13-23 GPa, the first syntheses of Na-rich hollandite and Na-rich CAS phase, and the discovery of two new  $\text{Al}_2\text{SiO}_5$  phases. All of these are described in this doctoral dissertation, although some of them are still in progress at present. I must work harder to finish the job, because I know a good completion of my research projects is the best way to show my deep appreciation for your great contribution, my supervisors, other GRC members, and also my family.

I may be able to graduate as a PhD soon, and the graduation will be another beginning of my life of research. I will keep on growing up, please continue keeping your eyes on me.

Thank you very much!

Youmo Zhou

2017.1.19

## Abstract

Shock metamorphism in meteorites provides evidence to support that some minerals in meteorites underwent high pressures and high temperatures during impact. Plagioclase is a typical constituent mineral in chondritic and Martian meteorites, and shock metamorphism of plagioclase has been widely discovered. Lingunite (aluminosilicate hollandite with ~ 80 mol % Na) is a typical shock-metamorphic phase of albitic plagioclase in strongly shocked meteorites, and has been frequently discovered in or adjacent to the shock veins. However, its formation condition remains unclear, and its formation mechanism is still under debate. Based on the flow textures of lingunite, some previous studies suggested that lingunite crystallized from molten plagioclase under high pressures (Gillet et al. 2000; Xie and Sharp 2004). Following this view, subsolidus and melting phase relations of two feldspathic compositions,  $K_{0.2}Na_{0.8}AlSi_3O_8$  and  $K_{0.05}Na_{0.85}Ca_{0.10}Al_{1.1}Si_{2.9}O_8$  (the latter is similar to that of the albitic plagioclase in meteorites), have been studied by multi-anvil experiments mainly at pressure-temperature (P-T) conditions of 22 GPa and 2273-2700 K, and the P-T conditions are typical for the shock veins in strongly shocked meteorites.

The high-pressure and high-temperature (HPHT) experiments using  $K_{0.2}Na_{0.8}AlSi_3O_8$  as starting materials yielded phase assemblages of hollandite + stishovite + jadeite or calcium ferrite-type  $NaAlSiO_4$  at 2273 K below or above 22 GPa, respectively. Hollandite single phase with a composition of  $K_{0.2}Na_{0.8}AlSi_3O_8$  was synthesized at 22 GPa and 2273 K. Partial melting of  $K_{0.2}Na_{0.8}AlSi_3O_8$  was achieved at ~ 23 GPa and 2575-2675 K. Stishovite is the liquidus phase, and jadeite is the solidus phase. Due to the melting, hollandite released  $NaAlSi_3O_8$  components, and a jadeitic melt and stishovite were formed. Large-sized (20-50  $\mu m$ ) hollandite grains with high Na contents of 63-82 mol % crystallized from the jadeitic melt during quenching.

The HPHT experiment using a starting material of  $\text{K}_{0.05}\text{Na}_{0.85}\text{Ca}_{0.10}\text{Al}_{1.1}\text{Si}_{2.9}\text{O}_8$  yielded a jadeite-bearing phase assemblage of jadeite + stishovite + hollandite + CAS phase at 22 GPa and 2273 K. Partial melting of  $\text{K}_{0.05}\text{Na}_{0.85}\text{Ca}_{0.10}\text{Al}_{1.1}\text{Si}_{2.9}\text{O}_8$  was achieved at 22 GPa and 2475-2700 K. The melting sequence is jadeite (the solidus phase), hollandite, CAS phase and finally stishovite (the liquidus phase). Melting of stishovite was not observed in the experiments, and melting of jadeite, hollandite and CAS phase probably produced jadeitic melts and stishovite. Hollandite could contain 74-80 mol % Na plus Ca at 22 GPa and 2273-2500 K. At 22 GPa and 2273 K, CAS phase could contain only 35 mol % Na plus K, and was just a minor phase in the subsolidus phase assemblage. In contrast, CAS phase could contain 62-71 mol % Na plus K at 22 GPa and 2475-2700 K, and became a major phase in the phase assemblages of partial melting. Na-rich hollandite ( $\text{Na}/(\text{K}+\text{Na}+\text{Ca})$ ,  $\sim 0.73$ ) and Na-rich CAS phase ( $\text{Na}/(\text{K}+\text{Na}+\text{Ca})$ ,  $\sim 0.69$ - $0.78$ ) crystallized from the jadeitic melt during quenching. In the sample recovered at 22 GPa and 2700 K, an intergrowth of CAS phase and stishovite was observed by Raman spectroscopy.

The experimental results indicate that both Na-rich hollandite and Na-rich CAS phase can form in albite compositions at 22 GPa in two ways: (1) equilibrium formation in the stability regions and (2) non-equilibrium formation as quench crystals during quenching. However, both subsolidus and melting phase relations of  $\text{K}_{0.05}\text{Na}_{0.85}\text{Ca}_{0.10}\text{Al}_{1.1}\text{Si}_{2.9}\text{O}_8$  can hardly elucidate the occurrence of lingunite in strongly shocked meteorites, although compositionally lingunite-like hollandite has been reproduced in this study. This is because lingunite-like hollandite is a minor phase in subsolidus phase assemblages of albitic plagioclase, and kinetic factors are required to be studied in order to interpret the dominant occurrence of lingunite in plagioclase-like grains, which has been frequently found in strongly shocked meteorites, if lingunite formed via solid-state transformation. On the other hand, if lingunite formed by liquid crystallization, CAS phase should occur as quench crystals together with lingunite, while no CAS phase has been found in the shock metamorphism of albitic plagioclase.

Plagioclase in Martian meteorites has labradoritic compositions (e.g.,  $\text{Ab}_{47}\text{An}_{51}\text{Or}_2$ ), and a shock-metamorphic phase assemblage of CAS phase plus stishovite has been discovered within labradorite-like grains in some Martian meteorites. In comparison to shock-metamorphic CAS phase, the quench-formed CAS phase observed in this study exhibits similar appearance under electron microscopic observation. The intergrowth of CAS phase and stishovite from the jadeitic melt in this study resembles the shock-metamorphic phase assemblage of CAS phase plus stishovite in some Martian meteorites. These similarities suggest that the CAS phase found in Martian meteorites probably formed through a similar mechanism of liquid crystallization, as proposed by Beck et al. (2004) and El Goresy et al. (2013). In this scenario, some labradoritic plagioclase was completely melted at 22 GPa above 2700 K during collision, and subsequently, CAS phase and stishovite crystallized from the labradoritic melt during quenching under high pressures. Furthermore, crystallization duration of CAS phase during collision might be at the same magnitude as that during quenching in the HPHT experiments of this study, based on the similarity in grain sizes between the shock-metamorphic CAS phase in Martian meteorites and the quench-formed CAS phase in this study.

An unknown  $\text{Al}_2\text{SiO}_5$  phase was encountered in the melting experiment of  $\text{K}_{0.2}\text{Na}_{0.8}\text{AlSi}_3\text{O}_8$  at 22.5 GPa and 2650 K. Subsequently, phase relations of  $\text{Al}_2\text{SiO}_5$  have been studied at 13-23 GPa and 2200-2800 K. The phase assemblage of corundum plus stishovite is stable at 14-23 GPa below 2500 K, and two novel  $\text{Al}_2\text{SiO}_5$  phases are stable above 2500 K at 14-17 and 17-23 GPa, respectively. Structural identification using X-ray and electron diffraction indicates that the new  $\text{Al}_2\text{SiO}_5$  phase stable at 17-23 GPa and above 2500 K has a  $\text{V}_3\text{O}_5$  structure (C2/m), and its lattice parameters have been preliminarily determined as  $a = 9.2964 \text{ \AA}$ ,  $b = 4.7068 \text{ \AA}$ ,  $c = 6.6272 \text{ \AA}$  and  $\beta = 111.30^\circ$ .

# Contents

## Chapter 1 Introduction

1.1 Constraints on the shock conditions of meteorites from static HPHT experiments .....	1
1.2 Shock metamorphism of plagioclase in the shock veins of strongly shocked meteorites ...	4
1.3 Phase transitions of feldspars at HPHT .....	7
1.4 Unclear points on the shock metamorphism of plagioclase and strategy of this study .....	9

## Chapter 2 Subsolidus phase relations in the system $\text{KAlSi}_3\text{O}_8\text{-NaAlSi}_3\text{O}_8$ at 20-23 GPa

2.1 Introduction .....	11
2.2 Experimental methods .....	12
2.3 Results and discussion .....	14
Tables and figures in <b>Chapter 2</b> .....	18

## Chapter 3

### Melting experiments of $\text{K}_{0.2}\text{Na}_{0.8}\text{AlSi}_3\text{O}_8$ and $\text{K}_{0.05}\text{Na}_{0.85}\text{Ca}_{0.10}\text{Al}_{1.1}\text{Si}_{2.9}\text{O}_8$ at ~ 22 GPa

3.1 Introduction .....	29
3.2 Experimental methods .....	29
3.3 Melting experiments of $\text{K}_{0.2}\text{Na}_{0.8}\text{AlSi}_3\text{O}_8$ at ~ 23 GPa .....	31
3.4 Subsolidus and melting experiments of $\text{K}_{0.05}\text{Na}_{0.85}\text{Ca}_{0.10}\text{Al}_{1.1}\text{Si}_{2.9}\text{O}_8$ at 22 GPa .....	36
3.5 Quench crystals obtained in the partial melting of $\text{K}_{0.2}\text{Na}_{0.8}\text{AlSi}_3\text{O}_8$ .....	40
3.6 Quench crystals obtained in the partial melting of $\text{K}_{0.05}\text{Na}_{0.85}\text{Ca}_{0.10}\text{Al}_{1.1}\text{Si}_{2.9}\text{O}_8$ .....	42
3.7 Implications for the shock metamorphism of plagioclase in strongly shocked meteorites	45
Tables and figures in <b>Chapter 3</b> .....	51

## Chapter 4 New high-pressure forms of $\text{Al}_2\text{SiO}_5$

4.1 Introduction .....	63
4.2 Experimental methods .....	64
4.3 Structural identification of new $\text{Al}_2\text{SiO}_5$ phases .....	65
4.4 Phase relations of $\text{Al}_2\text{SiO}_5$ at 13-23 GPa and 2200-2800 K .....	68
Tables and figures in <b>Chapter 4</b> .....	73

<b>References</b> .....	87
-------------------------	----

# Chapter 1

## Introduction

### 1.1 Constraints on the shock conditions of meteorites from static HPHT experiments

Collisions among celestial bodies have repeatedly occurred throughout the history of the solar system. The remaining small celestial bodies, asteroids, are accepted as the source of most meteorites. Since meteorites recorded much information about the ancient impacts, studies on meteorites are important to understand the impact history of the solar system.

The evidence of impact recorded in meteorites include fragmentation, deformation, defects in minerals, shock veins and shock metamorphism. Shock metamorphism is commonly discovered in or adjacent to the shock veins, and provides a clear evidence to support that a part of minerals in meteorites underwent high pressures and high temperatures during shock events. Recently, with the wide application of advanced micro-analytical techniques, like micro Raman spectroscopy and transmission electron microscopy, plenty of shock-metamorphic phases have been discovered. Based on the close observations of shock-metamorphic phases and the related phase relations determined using kinetic or static high-pressure and high-temperature (HPHT) experiments, the formation mechanisms of shock-metamorphic phases and the shock conditions have been widely discussed and estimated.

Stöffler et al. (1991) systematically studied the shock effects in olivine and plagioclase, and classified the shock stages of meteorites into six (S1-S6), among which the S6 stage (very strongly shocked) typically corresponds to the phase transformation of olivine into ringwoodite. Based on the classification of Stöffler et al. (1991), the meteorites containing ringwoodite were ever exposed to high pressures of 45-90 GPa. Meteorites at the S5 (with maskelynite) and S6 shock stages, which can be called “strongly shocked meteorites”, are mainly focused on, in this dissertation.



Shock veins, which were formed from a localized whole-rock melting resulted from a shear heating, are common in strongly shocked meteorites. Generally, shock veins contain two types of phase aggregates: (1) a fine-grained phase assemblage of aluminous garnet, magnesio-wüstite, Fe-Ni and/or FeS droplets, and (2) coarse-grained fragments of minerals entrained into the shock veins (e.g., Chen et al. 1996; Xie and Sharp 2007). The fine-grained phase assemblage of aluminous garnet plus magnesio-wüstite is considered to have crystallized from a whole-rock melt at 20-24 GPa and 2300-2500 K (Chen et al. 1996; Gillet et al. 2000), based on the melting phase relations of peridotite (Zhang and Herzberg 1994) and the Allende meteorite (Agee et al. 1995). The coarse-grained fragments of minerals are usually ringwoodite and akimotoite, which formed via solid-state transformation from the original olivine and enstatite, respectively, and the corresponding formation pressures are inferred to be 18-23 GPa (e.g., Chen et al. 2004b; Xie and Sharp 2004; Ohtani et al. 2004; Ozawa et al. 2009), mainly based on the subsolidus phase relations of  $\text{Mg}_2\text{SiO}_4\text{-Fe}_2\text{SiO}_4$  (e.g., Katsura and Ito 1989) and  $\text{MgSiO}_3$  (e.g., Sawamoto 1987), respectively.

For the same strongly shocked meteorites, the shock pressures inferred based on static HPHT experiments are much lower than those inferred based on shock experiments (e.g., Chen et al. 1996; Xie and Sharp 2004). Shock experiments have duplicated many shock-metamorphic features observed in meteorites, such as fragmentation and planar deformation features (PDFs), but none of high-pressure phases found in meteorites has been reproduced. The major limitation of shock experiments is the extremely short shock durations ( $< 10 \mu\text{s}$ ), and phase transitions of minerals, such as olivine and enstatite, will not occur within such short shock durations because of the sluggish kinetics (Sharp and DeCarli 2006). On the other hand, temperature effects were not discussed in the shock calibration of Stöffler et al. (1991). The samples used in most shock-recovery experiments are single crystals and igneous rock fragments, which are not porous, in contrast to the originally porous meteorites, and shock experiments on nonporous samples result

in relatively low shock temperatures (Sharp and DeCarli 2006). Schmitt (2000) experimentally demonstrated the importance of kinetics in shock metamorphism by the fact that the formation of maskelynite occurred at relatively low pressures of 20-25 GPa in the shock experiments at the elevated temperature of 920 K, compared with 25-30 GPa in the low-temperatures runs at 293 K and 35-45 GPa in the experimental study of Stöffler et al. (1991).

As mentioned above, none of high-pressure phases discovered in meteorites has been reproduced via shock experiments. In contrast, the most common phase assemblage in the shock veins, aluminous garnet plus magnesiowüstite, has been produced in static HPHT experiments on peridotite (Zhang and Herzberg 1994) and the Allende meteorite (Agee et al. 1995), and the samples recovered from experiments are texturally and compositionally similar to the observed shock veins of strongly shocked meteorites (e.g., Chen et al. 1996; Xie et al. 2001). Compared with the solid-state phase transitions in meteorites, the crystallization of shock veins involves much small kinetic barriers, and this is why high-pressure melting phase relations can be used to interpret the crystallization of shock veins (Sharp and DeCarli 2006). In the case of the solid-state phase transitions of olivine in meteorites, the intracrystalline ringwoodite transformation in olivine at 18-20 GPa and 1273-1673 K (Kerschhofer L et al. 1996; Kerschhofer L et al. 2000) resembles the ringwoodite lamellae observed in strongly shocked meteorites (e.g., Chen et al. 2004b; Ohtani et al. 2004).

Natural shock events could generate higher temperatures in meteorites during collision and last for longer durations than those in artificial shock events. The higher temperatures help to overcome the large activation barriers, and the longer durations are required for the formation of high-pressure phases with sluggish kinetics. Consequently, phase relations determined under static HPHT conditions describe the natural occurrence of high-pressure phases better than the shock effects studied in shock experiments, and can be used to preliminarily constrain the shock conditions of meteorites.

## **1.2 Shock metamorphism of plagioclase in the shock veins of strongly shocked meteorites**

Plagioclase is the third important constituent mineral in strongly shocked meteorites, in addition to olivine and enstatite. Based on plenty of reports, it is known that most plagioclase in strongly shocked meteorites has albitic compositions similar to  $Ab_{85}An_{10}O_5$  (Ab, albite; An, anorthite; Or, orthoclase) (Chen and El Goresy 2000; Gillet et al. 2000; Tomioka et al. 2000; Xie et al. 2001; Kimura et al. 2003; Ohtani et al. 2004; Miyahara et al. 2009; Ozawa et al. 2009; Miyahara et al. 2013a), and the plagioclase in Martian meteorites has labradoritic compositions similar to  $Ab_{47}An_{51}Or_2$  (Chen and El Goresy 2000; Langenhorst and Poirier JP 2000; Beck et al. 2004; El Goresy et al. 2013). The shock metamorphism of plagioclase is diverse and complex, and full of mysteries.

### **1.2.1 Maskelynite**

Maskelynite, the most common shock-metamorphic product of plagioclase in strongly shocked meteorites, refers to shock-induced amorphous plagioclase. However, the definition of “maskelynite” is still under debate. Researchers of shock experiments (e.g., Stöffler et al. 1991) believe that plagioclase in strongly shocked meteorites has two types of amorphization: (1) the solid-state transformation of plagioclase into diaplectic glass (maskelynite) and (2) the shock-induced melting of plagioclase and the subsequent formation of normal glass. However, Chen and El Goresy (2000) and El Goresy et al. (2013) pointed out that the maskelynite commonly observed in strongly shocked meteorites is not a diaplectic glass but a glass quenched from a shock-induced dense melt under high pressures, by summarizing and comparing the features of natural and artificial diaplectic glass and maskelynite. As summarized by El Goresy et al. (2013), “diaplectic glass is an amorphous mineral glass characterized by lack of evidence of melting or flow-features, accordingly lack of smooth surfaces in reflected light and BSE-SEM, but depicts shock-induced fractures and more importantly, planar elements or planar deformation features (PDFs) oriented along distinct crystallographic planes of the pre-amorphized grains; in contrast

to diaplectic glass, maskelynite has smooth surface appearance in reflected light consistent with a formation by melting and quenching under high pressures, thus welding and erasing all the preexisting cleavage, cracks, shock-induced fractures and PDFs". Detailed descriptions can be seen in Chen and El Goresy (2000).

Regardless of the debate on the nature of maskelynite, it is known based on plenty of reports that maskelynite in strongly shocked meteorites has similar compositions, relative to the original plagioclase, and exhibits smooth surfaces with much less cracks, in contrast to other minerals full of cracks (e.g., olivine and enstatite) (e.g., Gillet et al. 2000; Xie et al. 2001; Chen et al. 2004a; Xie et al. 2006; Miyahara et al. 2013a; Miyahara et al. 2013b).

### **1.2.2 Liebermannite and Lingunite**

$\text{KAlSi}_3\text{O}_8$  hollandite (K hollandite) is the high-pressure polymorph of orthoclase at 9-128 GPa (above  $\sim 20$  GPa, hollandite II, Ferroir et al. 2006) (Ringwood et al. 1967; Urakawa et al. 1994; Hirao et al. 2008). K hollandite has been named liebermannite, due to the discovery of  $\text{K}_{0.76}\text{Na}_{0.14}\text{Ca}_{0.02}\text{Al}_{1.03}\text{Si}_{3.00}\text{O}_8$  hollandite in the Martian meteorite Zagami (Langenhorst and Poirier 2000; Ma et al. 2015); Na hollandite has been named lingunite, due to the discovery of  $\text{K}_{0.08}\text{Na}_{0.80}\text{Ca}_{0.12}\text{Al}_{1.12}\text{Si}_{2.88}\text{O}_8$  hollandite in the Sixiangkou meteorite (Gillet et al. 2000).

Lingunite has been frequently discovered in or adjacent to the shock veins of strongly shocked meteorites, and shows similar compositions, relative to the original plagioclase (e.g., Mori 1994; Gillet et al. 2000; Tomioka et al. 2000; Ohtani et al. 2004; Ozawa et al. 2009). The lingunite in the Tenham meteorites is in form of aggregates of nanocrystals (up to  $\sim 100$  nm) (Tomioka et al. 2000; Xie and Sharp 2007); the lingunite in the Sixiangkou meteorite reveals a fine-grained network of bright and dark lamellae in maskelynite, and jadeite has also been found in maskelynite in some rare cases (Gillet et al. 2000); lamellae of lingunite and jadeite coexists with each other in the Yamato 74445 meteorite (Ozawa et al. 2009). The formation mechanism

of lingunite has been interpreted to be solid-state transformation (Tomiooka et al. 2000; Xie and Sharp 2007; Ozawa et al. 2009) or liquid crystallization (Gillet et al. 2000; Xie and Sharp 2004).

### **1.2.3 Jadeite**

Similar to lingunite, jadeite has also been discovered in or adjacent to the shock veins of strongly shocked meteorites (Gillet et al. 2000; Ohtani et al. 2004; Ozawa et al. 2009; Sharp et al. 2015). It was reported that the jadeite in the meteorites, Yamato 791384, 74445 and 75100 and Sahara 98222, shows albitic compositions, similar to the original plagioclase (Kimura et al. 2000; Ohtani et al. 2004; Ozawa et al. 2009). Miyahara et al. (2013a) reported that the jadeite in the meteorites Yamato 791384 and 75100 shows albitic compositions in electron microprobe analyses, but shows jadeitic compositions in TEM-EDS analyses. Jadeite is in form of lamellae in the Yamato 74445 meteorite, and is polycrystalline-like, particle-like and stringer-like in the Sahara 98222 meteorite (Ozawa et al. 2009); some albitic grains within the shock veins of the Yamato 791384 meteorite consist of jadeite nanocrystals (~ 200 nm) and amorphous materials.

No stishovite was detected in or around jadeite in strongly shocked meteorites (Kimura et al. 2000; Ohtani et al. 2004; Ozawa et al. 2009; Miyahara et al. 2013a). This is not consistent with the phase relations of albite (e.g., Akaogi et al. 2010). Kubo et al. (2010) studied kinetics of the formation of jadeite and stishovite in amorphous plagioclase by solid-state transformation, and elucidated the absence of stishovite in shock-metamorphic jadeite as a result of the sluggish crystallization kinetics of stishovite.

### **1.2.4 Na-rich CAS phase**

CAS phase, with a hexagonal barium ferrite-type structure (Gautron et al. 1999), was first observed by Irifune et al. (1994) in continental materials under P-T conditions of mantle transition zone. CAS phase was discovered in some Martian meteorites (El Goresy et al. 2013),

and the compositions are rich in Na, such as the  $K_{0.04}Na_{0.83}Ca_{0.29}Al_{2.91}Si_{2.95}O_{11}$  CAS phase in the Zagami meteorite (Beck et al. 2004). The plagioclase in Martian meteorites has labradoritic compositions (Chen and El Goresy et al. 2000; Langenhorst and Poirier 2000; Beck et al. 2004).

Na-rich CAS phase was observed to coexist with stishovite, and two textural settings of Na-rich CAS phase plus stishovite were found: (1) equant crystals of Na-rich CAS phase coexisting with stishovite clusters in a melt pocket of the Zagami meteorite (Beck et al. 2004) and (2) Na-rich CAS phase and stishovite, respectively, dominating two spatially separated distinct regions of the same large melt pool in the NWA856 meteorite (El Goresy et al. 2013). Na-rich CAS phase likely formed via liquid crystallization (Beck et al. 2004; El Goresy et al. 2013).

### **1.3 Phase transitions of feldspars at HPHT**

Phase relations of feldspar end-members and K-Na feldspar solid-solutions have been studied, which are important for understanding the shock metamorphism of plagioclase.

Orthoclase dissociates into a mixture of wadeite ( $K_2Si_4O_9$ ), kyanite and coesite at  $\sim 6.5$  GPa and 973-1673 K, and with increasing pressure, the mixture constitute K hollandite ( $KAl-Si_3O_8$ ) at 9 GPa and 973-1673 K (Yagi et al. 1994; Urakawa et al. 1994). K hollandite transforms into a monoclinic structure named hollandite II (Sueda et al. 2004) by a second-order transition at  $\sim 20$  GPa and room temperature (Ferroir et al. 2006), and the hollandite II phase is stable up to 128 GPa even at high temperatures (Hirao et al. 2008).

Albite dissociates into jadeite and quartz at 2.6-3.2 GPa and 1273-1673 K (e.g., Birch and LeComte 1960), and the phase assemblage of jadeite plus silica (e.g., Presnall 1995: up to  $\sim 3$  GPa, quartz; 3-9 GPa, coesite; above 9 GPa, stishovite) is stable up to  $\sim 22$  GPa at 1073-2273 K, and transforms into calcium ferrite-type  $NaAlSiO_4$  (Yamada et al. 1983) plus stishovite with further increasing pressure (Yagi et al. 1994; Akaogi et al. 2010). Liu (1978) and Liu and El Goresy (2007) reported that Na hollandite is stable in a narrow pressure range at  $\sim 21$  GPa

and 1273-1773 K. Tutti (2007) claimed that Na hollandite was found as a minor phase together with calcium ferrite-type  $\text{NaAlSiO}_4$  and stishovite in laser-heated albite at  $\sim 22.5$  GPa and 2273 K. However, Yagi et al. (1994) and Akaogi et al. (2010) did not recover any Na hollandite from an albite composition at 21-23 GPa and 1073-2273 K. Kawai and Tsuchiya (2013) predicted by ab initio calculation that Na hollandite is metastable.

K hollandite accommodates  $\text{NaAlSi}_3\text{O}_8$  component in the system  $\text{KAlSi}_3\text{O}_8$ - $\text{NaAlSi}_3\text{O}_8$  above 9 GPa, and the excessive  $\text{NaAlSi}_3\text{O}_8$  component relative to the solubility of  $\text{NaAlSi}_3\text{O}_8$  component in hollandite exists in form of jadeite plus stishovite below  $\sim 22$  GPa or calcium ferrite-type  $\text{NaAlSiO}_4$  plus stishovite above  $\sim 22$  GPa (Yagi et al. 1994). The solubility of  $\text{NaAlSi}_3\text{O}_8$  component in hollandite increases with increasing pressure up to  $\sim 22$  GPa, and decreases significantly after the dissociation of jadeite into calcium ferrite-type  $\text{NaAlSiO}_4$  plus stishovite (Yagi et al. 1994). Liu (2006) reported that the solubility of  $\text{NaAlSi}_3\text{O}_8$  component in hollandite positively correlates with temperature. However, the maximal solubility of  $\sim 51$  mol % reported by Liu (2006) at  $\sim 22$  GPa and 2473 K is not so different from the value of 40 mol % reported by Yagi et al. (1994) at  $\sim 22$  GPa and 1273 K, or the values of  $\sim 50$  mol % reported by Akaogi et al. (2005) and Liu et al. (2005) at  $\sim 22$  GPa and 1673 and 1973 K, respectively.

Anorthite dissociates into a mixture of grossular garnet, kyanite and quartz at 2-3 GPa and 1273-1673 K (e.g., Presnall 1995), and the phase assemblage of grossular garnet + kyanite + silica (e.g., Presnall 1995: up to  $\sim 3$  GPa, quartz; 3-9 GPa, coesite; above 9 GPa, stishovite) is stable up to 12-14 GPa at 1673-1773 K, and is replaced by the phase assemblage of grossular garnet + CAS phase + stishovite (Gautron et al. 1996); the latter phase assemblage is stable up to  $\sim 20$  GPa at 1673-2473 K, and then transforms into the phase assemblage of Ca perovskite + CAS phase + stishovite above  $\sim 20$  GPa at 1673-2473 K (Liu et al. 2012). The stability region of the phase assemblage of Ca perovskite + kyanite +  $\text{Ca}_{1.33}\text{Al}_{1.33}\text{Si}_{2.33}\text{O}_8$  hollandite reported by Gautron and Madon (1994) was not reproduced in the experiments of Gautron et al. (1996) and Liu et al. (2012).

#### **1.4 Unclear points on the shock metamorphism of plagioclase and purpose of this study**

Although mechanisms of the shock metamorphism of plagioclase in strongly shocked meteorites have been widely discussed, discrepancies and suspicious points can be easily found among previous experimental and observation studies.

The shock metamorphism of albitic plagioclase, including maskelynite, lingunite and jadeite, mostly shows similar appearance. Sharp and DeCarli (2006) mentioned that “optically, the hollandite-structured plagioclase is isotropic and looks like maskelynite (diaplectic glass) or melted plagioclase (normal glass)”. On the other hand, coexistence among lingunite, jadeite and maskelynite has been repeatedly reported (Gillet et al. 2000; Kimura et al. 2000; Ozawa et al. 2009; Miyahara et al. 2013a; Sharp et al. 2015). Therefore, it is quite difficult to understand why lingunite and jadeite formed from plagioclase via solid-state transformation (e.g., Tomioka et al. 2000; Kubo et al. 2010), while maskelynite is a quench product of plagioclase melt under high pressures (Chen and El Goresy 2000; El Goresy et al. 2013).

Recently, Ozawa et al. (2014) reported a formation of needle-like or skeletal-rhombic grains of jadeite from an albitic melt in the Chelyabinsk meteorite; Ma et al. (2015) discovered a new vacancy-rich and high-pressure clinopyroxene named tissintite together with labradoritic maskelynite in the Martian meteorite Tissint, and proposed that tissintite formed as the liquidus phase in a labradoritic melt, solely based on the phase diagram of albite. The SEM images given by Ozawa et al. (2014) and Ma et al. (2015) clearly show coexistence of pyroxenes (jadeite and tissintite, respectively) and maskelynite, and the maskelynite also looks like those coexisting with lingunite and/or jadeite (e.g., Gillet et al. 2000; Miyahara et al. 2013a). If these pyroxenes formed via liquid crystallization, as suggested by Ozawa et al. (2014) and Ma et al. (2015), why did the lingunite and jadeite within similar maskelynite form via solid-state transformation?

To discuss the formation mechanisms of lingunite and jadeite, previous studies focused on the micro textures and the compositions. However, as mentioned above, the appearance of



maskelynite, lingunite and jadeite looks similar. Some TEM observations reveal nanocrystals of lingunite, and the granular polycrystalline textures of lingunite can be consistent with either solid-state transformation or liquid crystallization (Xie and Sharp 2004; Xie and Sharp 2007). Almost all the previous studies reported that lingunite has similar compositions, relative to the original plagioclase. However, the compositions of lingunite are likely bulk compositions, since the grain sizes of lingunite are too small for EPMA analysis. Similarly, the grain sizes of shock-metamorphic jadeite and Na-rich CAS phase are also insufficient for EPMA analysis (Beck et al. 2004; El Goresy et al. 2013; Miyahara et al. 2013a). Relative to the shock metamorphism of olivine and enstatite, not much information is available for inferring the formation mechanism of lingunite and jadeite.

On the other hand, phase relations of feldspar end-members and K-Na feldspar solid-solutions equilibrated under subsolidus conditions in previous experimental studies are unable to explain the occurrence of maskelynite and lingunite and the absence of stishovite in the shock metamorphism of albitic plagioclase. Only a few studies (Kubo et al. 2010; Kubo et al. 2016) started to investigate kinetic factors in the shock metamorphism of plagioclase.

In this study, following the descriptions of maskelynite made by Chen and El Goresy (2000) and El Goresy et al. (2013), multi-anvil HPHT experiments have been made to test the possibility that nature of the shock metamorphism of plagioclase in strongly shocked meteorites is shock-induced melting and subsequent liquid crystallization. For this purpose, subsolidus and melting phase relations of the typical albitic composition ( $\text{Ab}_{85}\text{An}_{10}\text{Or}_5$ ) observed in meteorites have been investigated at the typical P-T conditions of shock veins, ~ 22 GPa and 2200-2700 K. Particularly, the stability regions and occurrence of lingunite and Na-rich CAS phase have been clarified, which help much to understand the natural occurrence of lingunite and Na-rich CAS phase in strongly shocked meteorites. To make clear definitions, “lingunite” refers to the Na-rich hollandite found in meteorites, and “Na-rich hollandite” is the experimental product.

## Chapter 2

### Subsolidus phase relations in the system $\text{KAlSi}_3\text{O}_8$ - $\text{NaAlSi}_3\text{O}_8$ at 20-23 GPa

#### 2.1 Introduction

As mentioned in **Section 1.2.2** and **1.3**, lingunite is a typical shock-metamorphic phase of plagioclase, and is usually rich in Na. In contrast to the frequent discovery of lingunite in the shock veins of meteorites, hollandite with a Na content higher than 50 mol % has not yet been synthesized. Liu (1978) and Tutti (2007) reported the synthesis of Na hollandite at  $\sim 22$  GPa and  $\sim 1273$  and  $2273$  K, respectively, while neither of them provided clear evidence from XRD to support the formation of Na hollandite in their DAC experiments, because of the considerable overlapping among the XRD peaks of hollandite, calcium ferrite-type  $\text{NaAlSiO}_4$  (or jadeite), and stishovite. On the other hand, the stability regions of Na hollandite proposed by Liu (1978), Liu and Goresy (2007) and Tutti (2007) were not reproduced by Yagi et al. (1994) and Akaogi et al. (2010). Several previous studies (Irifune et al. 1994; Yagi et al. 1994; Akaogi et al. 2005; Liu et al. 2005; Ishii et al. 2012) demonstrated that the solubility of  $\text{NaAlSi}_3\text{O}_8$  in hollandite is up to 50 mol % at 16-23 GPa and temperatures up to 2073 K in the system  $\text{KAlSi}_3\text{O}_8$ - $\text{NaAlSi}_3\text{O}_8$  and continental materials. Liu (2006) studied the phase relations in the system  $\text{KAlSi}_3\text{O}_8$ - $\text{NaAlSi}_3\text{O}_8$  at 14-25 GPa and 1673-2673 K, and showed that the solubility of  $\text{NaAlSi}_3\text{O}_8$  in hollandite positively correlates with temperature. However, it can be found that the hollandite obtained at 22 GPa and 2273-2473 K in the experiments of Liu (2006) contains 40-50 mol % Na, showing no compositional difference in comparison to those obtained at similar pressures but relatively low temperatures below 2073 K in other previous studies. This likely suggests that the positive temperature dependence of the solubility of  $\text{NaAlSi}_3\text{O}_8$  in hollandite shown by Liu (2006) does not reveal the real situation. Therefore, in this chapter, phase relations in the system  $\text{KAlSi}_3\text{O}_8$ - $\text{NaAlSi}_3\text{O}_8$  has been studied to clarify the effects of pressure and temperature on the solubility of  $\text{NaAlSi}_3\text{O}_8$  in hollandite, particularly focusing those at 20-23 GPa and 1873 and 2273 K.

## 2.2 Experimental methods

### 2.2.1 Starting materials

The starting materials are feldspathic glasses with compositions of  $K_{0.45}Na_{0.55}AlSi_3O_8$  and  $K_{0.2}Na_{0.8}AlSi_3O_8$ . To prepare homogenous glasses, mixtures of stoichiometrically weighed chemicals,  $K_2CO_3$ ,  $Na_2CO_3$ ,  $Al_2O_3$  and  $SiO_2$ , were first heated at 1273 K for 12 hours to remove  $CO_2$  and then melted twice in home-made Pt crucibles at 2000 K for 1 hour. About 15 mol %  $K_2CO_3$  was added into the chemical mixtures in advance to compensate the loss of K during heating. Transparent glasses with bubbles were obtained by air quenching, and the compositions were measured by electron probe micro-analysis. **Table 2.1** lists compositions of the feldspathic glasses. The glasses were crushed and ground, and then stored at 383 K before being used.

### 2.2.2 HPHT experiments

The HPHT experiments were performed in the Kawai-type multi-anvil high-pressure apparatuses (Orange 1000 and 2000) installed at Geodynamics Research Center (GRC), Ehime University. The pressure medium was an octahedron of Co-doped MgO with an edge length of 10 mm, and the truncation edge length of the tungsten-carbide anvil was 4 mm. The material of heater was  $LaCrO_3$ . MgO and  $ZrO_2$  were used as electrical and thermal insulators surrounding Pt capsules and Mo electrodes, respectively. The schematic diagram of the 10/4 cell assembly is shown in **Figure 2.1a**.

Pressures at room temperature were calibrated by observing the diagnostic changes in the resistances of ZnTe (9.6 and 12.0 GPa), ZnS (15.5 GPa) and GaAs (18.3 GPa) induced by the semiconductor-metal transitions under high pressures. Pressures at 1873 K were estimated by the phase transitions of  $Mg_2SiO_4$  between forsterite and wadsleyite at 15.0 GPa (Morishima et al. 1994),  $Mg_2SiO_4$  between wadsleyite and ringwoodite at 21.4 GPa (Suzuki et al. 2000) and  $MgSiO_3$  between akimotoite and bridgmanite at 22.3 GPa (Fei et al. 2004). **Figure 2.2** shows

the pressure calibrations at room temperature and 1873 K. Pressures at 2273 K were estimated by the phase transitions of  $\text{MgSiO}_3$  between majorite and bridgmanite at 21.5 GPa (Fei et al. 2004) and the decomposition of  $\text{Mg}_2\text{SiO}_4$  into bridgmanite and periclase at 23.0 GPa (Fei et al. 2004). The temperature was monitored by a  $\text{W}_{97}\text{Re}_3$ - $\text{W}_{75}\text{Re}_{25}$  thermocouple. No correction was made for the pressure effect on the electromotive force of the thermocouple.

In most of the HPHT experiments, the temperature was increased to the target value in 20 minutes, and the heating was kept for 12 hours and subsequently stopped by cutting off the power supply. It was found that compositional zoning usually occurred in the hollandite grains, when the heating durations were relatively short (e.g., 2 hours), in the HPHT experiments above 20 GPa. The samples heated for 9 and 12 hours comprise compositionally homogeneous grains with sharp boundaries, indicating that the durations of 9 and 12 hours used in most of the HPHT experiments were sufficient for phase equilibrium.

### **2.2.3 Analytical methods**

Samples recovered from the HPHT experiments were embedded in epoxy resin and polished for subsequent analyses. Phase identification was performed by a micro-focus X-ray diffraction (XRD) apparatus (Rigaku MicroMax-007HF) using  $\text{Cu K}\alpha$  radiation. For electron microscopic observation and compositional analysis, the samples were coated with osmium. In the case of carbon coating, uncertainties in the thickness of the coating layer may result in some variations in the quantitative values of elements and the weight totals. These variations can be reduced by using osmium coating instead, because the thickness of the osmium coating layer can be precisely controlled, which enables precise absorption corrections for the coating layer (Ohfuji and Yamamoto 2015). Micro textures of the samples were observed in a field-emission scanning electron microscope (FESEM, JEOL JSM7000F), and compositions of the samples were measured using an energy dispersive X-ray spectrometer (EDS, Oxford Instruments X-

Max<sup>N</sup>) attached to the FESEM with working parameters of 15 kV, 1 nA and collection times of 30-50 s. Albite was used as the standard for Na, Al and Si, and adularia was used for K. To avoid the serious evaporation of K and Na from the irradiated samples, compositional analysis in area mode was used, when measuring the feldspar standard samples and the glassy starting materials; point analysis was used when measuring the recovered samples. The EDS data were processed by the software Aztec (Oxford Instruments Nanotechnology Tools Ltd.) using the XPP method.

### 2.3 Results and discussion

**Table 2.2** lists conditions and results of the HPHT experiments performed at pressures of 20-23 GPa and temperatures of 1873 and 2273 K. Compositions of hollandite and some other phases (jadeite, calcium ferrite-type NaAlSiO<sub>4</sub> and stishovite) are shown in **Table 2.3** and **2.4**, respectively.

**Figure 2.3** shows micro textures of some typical samples with bulk compositions of K<sub>0.2</sub>Na<sub>0.8</sub>AlSi<sub>3</sub>O<sub>8</sub>. K-bearing hollandite can be recognized by its high brightness and elongated shape, and jadeite, calcium ferrite-type NaAlSiO<sub>4</sub> (CF) and stishovite are dark. Jadeite behaves as a matrix with inserted hollandite and stishovite grains in the phase assemblage of hollandite + jadeite + stishovite (**Figure 2.3a** and **2.3d**). In **Figure 2.3b**, except hollandite and one marked grain of CF, the matrix is dominated by tiny stishovite and CF, grain boundaries of which are hardly recognizable. **Figure 2.3c** is a magnification of the same sample shown in **Figure 2.3b**, revealing a texture composed of submicron stishovite and nanocrystals of CF. The duration of 12 hours was insufficient for the grain growth of CF and stishovite at 23 GPa and 1873 K. Yagi et al. (1994) and Akaogi et al. (2010) also observed tiny CF grains in their samples obtained at 23 GPa. The CF grains obtained at 23 GPa and 2273 K have large sizes up to 10 μm (**Figure 2.3f**). Comparing **Figure 2.3a** and **2.3b** with **Figure 2.3d** and **2.3f**, respectively, it is found that

the volume fraction of hollandite increases with increasing temperature from 1873 to 2273 K at the same pressures, which is due to the fact that the hollandite obtained at 2273 K possesses more Na, in comparison to those obtained at 1873 K and the same pressures (**Table 2.3**).

**Figure 2.4** shows XRD patterns of some typical samples, including the typical phase assemblages obtained in the HPHT experiments. High-pressure phase relations in the system  $\text{KAlSi}_3\text{O}_8$ - $\text{NaAlSi}_3\text{O}_8$  at 1873 and 2273 K (**Figure 2.5a** and **2.5b**) are modally consistent with those at 1273 K (Yagi et al. 1994): hollandite + jadeite + stishovite below 22 GPa, hollandite + CF + stishovite above 22 GPa, and hollandite in the single-phase region; the solubility of Na in hollandite increases with increasing pressure up to 22 GPa, and decreases significantly after the dissociation of jadeite into CF and stishovite, since the calcium ferrite structure is more capable of accommodating Na than the hollandite structure (Yamada et al. 1984). **Figure 2.5c** shows a positive temperature dependence of the solubility of Na in hollandite, in addition to the equally significant pressure effect that the solubility of Na in hollandite varies significantly in the range of 20-23 GPa, and the dissociation of jadeite changes the change trend of the solubility of Na in hollandite from increase to decrease. The hollandite synthesized at 22 GPa and 2273 K using the starting material of  $\text{K}_{0.2}\text{Na}_{0.8}\text{AlSi}_3\text{O}_8$  (**Figure 2.3e**) is almost a single phase with 79 mol % Na, similar to lingunite in terms of the Na content, and its XRD pattern (**Figure 2.4b**) reveals the existence of stishovite in trace amounts. Jadeite dissociated into CF and stishovite at ~ 22 GPa at 1873 and 2273 K, consistent with the results of Akaogi et al. (2010). However, in this study, the Clapeyron slope of jadeite dissociation is not discussed, since more accurate data are needed to check the plausible temperature dependence of jadeite dissociation given by Yagi et al. (1994) and Akaogi et al. (2010). Based on the compositional analyses (**Table 2.4**), jadeite and CF are stoichiometric, and the K contents in jadeite and CF are below the detection limit; stishovite contains a small amount of  $\text{Al}_2\text{O}_3$  (< 2 wt %).

Considering the positive temperature dependence shown in **Figure 2.5c**, Na hollandite is likely stable around 22 GPa only at temperatures above 2273 K. It is possible that the Na hollandite found by Liu (1978) and Tutti (2007) in the DAC experiments formed locally at some hot spots of laser heating where the temperatures were underestimated. Kawai and Tsuchiya (2013) predicted that Na hollandite is metastable through ab initio calculation, although the calculation was conducted at 0 K.

**Figure 2.5b** shows that the results of this study are quite different from those of Liu (2006). The data of Liu (2006) may match the results of this study, if the former moves down to lower pressures. This discrepancy is likely due to the fact that Liu (2006) did not do pressure calibrations at high-temperature conditions. Liu (2006) suggested that pressure is unimportant to the solubility of Na in hollandite at 22 and 25 GPa, because the latter had no large variation at 1673-2273 K in his study. However, it can be clearly seen from the results of Liu (2006) that the phase assemblage at 22 GPa is “hollandite II” (to be discussed later) + jadeite + stishovite, and the phase assemblage at 25 GPa is “hollandite II” + CF + stishovite. Using two data across a pressure interval of 3 GPa, Liu (2006) did not find the significant change of the solubility of Na in hollandite before and after the dissociation of jadeite into CF and stishovite, which can be seen in Yagi et al. (1994), Ishii et al. (2012) and this study, and therefore underestimated the solubility of Na in hollandite.

K hollandite transforms to a monoclinic structure named hollandite II (Sueda et al. 2004) via a second-order phase transition at ~ 20 GPa at room temperature (Ferroir et al. 2006). Liu (2006) hypothetically modified the phase relations in the system  $\text{KAlSi}_3\text{O}_8$ - $\text{NaAlSi}_3\text{O}_8$  by taking the hollandite-hollandite II transition into account, but no evidence was given to prove the occurrence of the unquenchable hollandite II phase in his products recovered from HPHT conditions, and also the effects of temperature and Na substitution on the hollandite-hollandite II transition were out of consideration. According to the Clapeyron slope reported by Nishiyama

et al. (2005), pressures of the previous (Yagi et al. 1994; Liu 2006) and present experiments are insufficient to trigger the hollandite-hollandite II transition at high-temperature conditions. On the other hand, the effect of Na substitution was studied merely by some theoretical calculations (Boffa Ballaran et al. 2009; Caracas and Boffa Ballaran 2010; Kawai and Tsuchiya 2013), and is still unclear. Thus, it is unreasonable to accept both the phase relations reported by Liu (2006) and the maximal solubility of Na in hollandite estimated by Liu (2006) based on the hollandite-hollandite II transition at 20-25 GPa and 1673-2273 K. In this study, the phase relations without the hollandite II phase are presented, based on the phase identification of the samples recovered from HPHT conditions. Studies using in situ X-ray observation are required to investigate the hollandite-hollandite II transition in the system  $\text{KAlSi}_3\text{O}_8\text{-NaAlSi}_3\text{O}_8$  under HPHT conditions.

Lattice parameters and unit cell volumes of hollandite were calculated using 10-25 XRD peaks in a two-theta range of 15-100 degree. The calculated results are listed in **Table 2.5** and plotted as functions of Na content in **Figure 2.6**. The lengths of a and c axes and the unit cell volume decrease with increasing Na content, because of replacing K (ion radius, 1.33 Å) by relatively small Na (ion radius, 0.95 Å). The linearly fitted lattice parameters and unit cell volume of hollandite are  $a$  (Å) =  $9.3302(22) - 0.0795(45) \times X_{\text{Na}}$ ,  $c$  (Å) =  $2.7260(4) - 0.0147(9) \times X_{\text{Na}}$  and  $V$  (Å<sup>3</sup>) =  $237.303(94) - 5.297(196) \times X_{\text{Na}}$ , where  $X_{\text{Na}}$  is Na/(K+Na). It can be seen from **Figure 2.6** that the lattice parameters of K hollandite in this study are comparable to those of Yagi et al. (1994), but the extrapolations of lattice parameters to Na hollandite in this study deviate from those of Yagi et al. (1994). Analytical uncertainties in XRD analysis likely affected their results, since only four data of lattice parameters of hollandite with Na contents lower than 40 mol % were used for the linear regressions. **Figure 2.6** also shows lattice parameters of the  $\text{Na}_{0.80}\text{Ca}_{0.12}\text{K}_{0.08}\text{Al}_{1.12}\text{Si}_{2.88}\text{O}_8$  lingunite (Gillet et al. 2000) for comparison. The length of its a axis matches the results of this study, while that of its c axis is obviously smaller.



## Chapter 3

### Melting experiments of $\text{K}_{0.2}\text{Na}_{0.8}\text{AlSi}_3\text{O}_8$ and $\text{K}_{0.05}\text{Na}_{0.85}\text{Ca}_{0.10}\text{Al}_{1.1}\text{Si}_{2.9}\text{O}_8$ at ~ 22 GPa

#### 3.1 Introduction

As mentioned in **Section 1.4**, mechanisms of the shock metamorphism of plagioclase in strongly shocked meteorites, solid-state transformation or liquid crystallization, are under debate. The shock-metamorphic products of albitic plagioclase, including lingunite, jadeite and maskelynite, entrained in or adjacent to the shock veins are large polycrystalline grains, similar to those of olivine and enstatite (Chen et al. 1996; Tomioka et al. 2000; Xie and Sharp 2007). Thus, the lingunite and jadeite found in maskelynite likely formed by solid-state transformation, like ringwoodite and akimotoite (e.g., Tomioka et al. 2000; Xie and Sharp 2007; Ozawa et al. 2009), otherwise it would be expected that the albitic melt did not mix with the surrounding chondritic melt (Sharp and DeCarli 2006). On the other hand, the shock-metamorphic products of albitic plagioclase show some evidence of melting (Chen and El Goresy 2000; Gillet et al. 2000; Xie and Sharp 2004; Miyahara et al. 2013). Kubo et al. (2010, 2016) studied the kinetics about the amorphization of albitic plagioclase and the crystallization of jadeite, stishovite and hollandite from the amorphized albitic plagioclase, and proposed the occurrence of jadeite and lingunite via solid-state transformation in amorphized albitic plagioclase. In contrast, melting experiments of  $\text{K}_{0.2}\text{Na}_{0.8}\text{AlSi}_3\text{O}_8$  and  $\text{K}_{0.05}\text{Na}_{0.85}\text{Ca}_{0.10}\text{Al}_{1.1}\text{Si}_{2.9}\text{O}_8$  have been performed in this chapter to test the possibility that the lingunite found in strongly shocked meteorites formed by liquid crystallization under high pressures.

#### 3.2 Experimental methods

##### 3.2.1 Starting materials

The starting materials are feldspathic glasses with compositions of  $\text{K}_{0.2}\text{Na}_{0.8}\text{AlSi}_3\text{O}_8$

and  $\text{K}_{0.05}\text{Na}_{0.85}\text{Ca}_{0.10}\text{Al}_{1.1}\text{Si}_{2.9}\text{O}_8$ . The preparation of glasses is described in **Section 2.2.1**, and  $\text{CaCO}_3$  was used when making the Ca-containing glass. Compositions of the feldspathic glasses are listed in **Table 2.1**. The glasses were crushed and ground, and then stored at 383 K before being used.

### 3.2.2 HPHT experiments

The multi-anvil high-pressure apparatuses mentioned in **Section 2.2.2** were used for the HPHT experiments.

To safely generate high temperatures up to 3000 K, the 10/4 cell assembly mentioned in **Section 2.2.2** was modified as follows: the outer and inner diameters of the  $\text{LaCrO}_3$  heater were reduced from 3 and 2 millimeters (**Figure 2.1a**) to 2.5 and 1.6 millimeters (**Figure 2.1b**, **2.1c** and **2.1d**), respectively; Re or graphite (surrounded by Re foil) capsules (**Figure 2.1b**, **2.1c** and **2.1d**) were used instead of Pt capsules (**Figure 2.1a**).

The pressure calibration follows those mentioned in **Section 2.2.2**. Due to the lack of pressure markers available for HPHT quench-recovery experiments at high temperatures above 2273 K, the pressure calibration at 1873 K (**Figure 2.2**) was used to estimate the pressures of the melting experiments. The temperature was monitored by a  $\text{W}_{97}\text{Re}_3$ - $\text{W}_{75}\text{Re}_{25}$  thermocouple. No correction was made for the pressure effect on the electromotive force of the thermocouple.

### 3.2.3 Analytical methods

Structural, morphological and compositional analyses using XRD, FESEM and EDS, respectively, are basically the same as those mentioned in **Section 2.2.3**.

In the compositional analysis, jadeite was quantified using the standards of jadeite (Na, Al and Si) and wollastonite (Ca), and other phases including solid phases and quench crystals were quantified using albite (Na, Al and Si), adularia (K) and wollastonite (Ca).

A laser Raman spectrometer (Jasco NRS-5100gr, laser wave-length 532 nm) was also utilized for structural analysis, especially for quench crystals. Each of the measurements lasted 120-300 s with a power of 5.6 mW.

### 3.3 Melting experiments of $\text{K}_{0.2}\text{Na}_{0.8}\text{AlSi}_3\text{O}_8$ at ~ 23 GPa

Three experimental runs were performed at ~ 23 GPa and ~ 2600 K using the starting material of  $\text{K}_{0.2}\text{Na}_{0.8}\text{AlSi}_3\text{O}_8$ . **Table 3.1** lists the experimental conditions and results. **Table 3.2** lists compositions of the recovered products. The starting materials were partially melted in the three runs, as shown in **Figure 3.1**, and the samples exhibit typical layered textures of partial melting, which reflect the thermal gradient through the capsule. **Figure 3.2** shows the samples in detail. Quench crystals accumulate at the hottest part of each capsule, which were formed by the rapid crystallization of melt during quenching. Stishovite is the liquidus phase followed by hollandite. It is unclear why there is no stishovite at the interface between the solid phases and the quench crystals in Run OS2813 (**Figure 3.2c**). **Table 3.2** shows that the melt of Run OS2809 and OS2835 has jadeitic compositions, and that of Run OS2813 is slightly depleted in Al; in comparison to the starting material, the melt has enlarged Na/(K+Na) ratios (~ 0.93), while the hollandite adjacent to the melt is depleted in Na (Na/(K+Na) ratios, 0.44-0.57).

An unknown  $\text{Al}_2\text{SiO}_5$  phase was found at the low-temperature (low-T) region of Run OS2809 (**Figure 3.2b**), which has been identified to be  $\text{V}_3\text{O}_5$  type (**Figure 3.3b**). The structural identification is described in **Chapter 5**. With decreasing temperature from 2650 to 2575 K at 22.5 GPa, jadeite appeared at the coldest part of Run OS2813 (**Figure 3.2d**). This indicates that jadeite is the solidus phase in the phase assemblage of hollandite + jadeite + stishovite. A grain of corundum was also found at the coldest part of Run OS2813 (**Figure 3.2d**), indicating that the starting material has slightly excessive  $\text{Al}_2\text{O}_3$  component, which resulted in the occurrence of  $\text{V}_3\text{O}_5$ -type  $\text{Al}_2\text{SiO}_5$  in Run OS2809. It is in agreement with the phase relations of  $\text{Al}_2\text{SiO}_5$

studied in **Chapter 5** that  $V_3O_5$ -type  $Al_2SiO_5$  was stabilized at the relatively high-T condition of Run OS2809, while corundum coexisted with stishovite at the relatively low-T condition of Run OS2813.

Considering the melting sequence of (1) jadeite, (2) hollandite and (3) stishovite and the compositions of melt and hollandite at the high-T regions, the partial melting of  $(K_{0.2}Na_{0.8})-AlSi_3O_8$  at 22.5 GPa can be described by **Reaction (1)**. In addition, **Reaction (2)** also makes sense. The melting behavior of  $K_{0.2}Na_{0.8}AlSi_3O_8$  at 22.5 GPa is, to some extent, similar to those of continental materials and a dry K-rich basaltic composition reported by Irifune et al. (1994) and Wang and Takahashi (1999), respectively, that K is more compatible than Na at  $\sim 22$  GPa, and stishovite is the liquidus phase followed by hollandite.

Na-rich hollandite + jadeite + stishovite  $\rightarrow$  Na-depleted hollandite

+ a jadeitic melt + stishovite ... **(1)**

Na-rich hollandite  $\rightarrow$  Na-depleted hollandite + a jadeitic melt + stishovite ... **(2)**

An unknown  $K_{0.04}Na_{1.00}Al_{2.94}Si_{3.04}O_{11}$  phase was observed at the low-T region of Run OS2835 (**Figure 3.2f**), together with hollandite, jadeite and stishovite. The corresponding XRD pattern (**Figure 3.3c**) shows that the peaks except those of hollandite, jadeite, stishovite and Re (capsule material) can be indexed to the structure of Ca-CAS phase clarified by Gautron et al. (1999). It was found that the XRD peaks of the observed CAS phase shift to high angles relative to those of Ca-CAS phase, which is probably due to the compositional difference between the  $K_{0.04}Na_{1.00}Al_{2.94}Si_{3.04}O_{11}$  phase and Ca-CAS phase ( $CaAl_4Si_2O_{11}$ ). The Raman spectrum of the  $K_{0.04}Na_{1.00}Al_{2.94}Si_{3.04}O_{11}$  phase (**Figure 3.8b**) exhibits vibration modes similar to those of Ca-CAS phase reported by Beck et al. (2004) and Zhai and Ito (2008). The vibration modes at 297, 640, 872 and 925  $cm^{-1}$  correspond to those of Ca-CAS phase at 280, 616, 851 and 910  $cm^{-1}$  in Beck et al. (2004) and at 290, 624, 855 and 910  $cm^{-1}$  in Zhai and Ito (2008), respectively. The compositional difference is also likely the reason to the differences in Raman shift between the

$K_{0.04}Na_{1.00}Al_{2.94}Si_{3.04}O_{11}$  phase and Ca-CAS phase. Thus, the  $K_{0.04}Na_{1.00}Al_{2.94}Si_{3.04}O_{11}$  phase is confirmed to be the Na end-member of CAS phase with an ideal composition of  $NaAl_3Si_3O_{11}$  (Akaogi et al. 2010). The vibration modes of hollandite and stishovite in the Raman spectrum of the Na-CAS phase likely derived from the neighboring grains of hollandite and stishovite. In addition, the non-ideal Al and Si numbers of the Na-CAS phase are likely attributed to the inappropriate employment of compositional standards.

In this study, Na-CAS phase formed in an albitic composition. It can be expected that some components rich in Na, Si and O must have been separated from the albitic composition, and the rest part could form the more Al-rich Na-CAS phase. El Goresy et al. (2013) speculated **Reaction (3)** to explain the formation of Na-CAS phase in labradoritic-albitic compositions in strongly shocked meteorites.

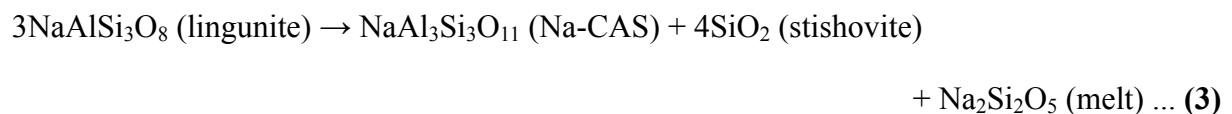


**Figure 3.4** clearly shows that the Na-CAS phase is more close to the high-T region of the capsule, compared with the jadeite located at the coldest part, suggesting the formation of Na-CAS phase from jadeite at elevated temperatures, as described by **Reaction (4)**.



It can be expected that stishovite has no contribution to the formation of Na-CAS phase from jadeite. Also, the obtained Na-CAS phase contains trace K, suggesting that the  $KAlSi_3O_8$  component in the starting material might have a very limited contribution to the formation of Na-CAS phase. The Na-rich melt generated by the formation of Na-CAS phase is supposed to have mixed with the melt at the hottest part of the capsule.

Na-CAS phase is likely stable in a narrow pressure range around 22 GPa above 2473 K, based on the positive temperature dependence of the solubility of  $NaAl_3Si_3O_{11}$  component

in CAS phase reported by Akaogi et al. (2010), although they did not expect a stability region of Na-CAS phase.

It is proposed that the occurrence of Na-CAS phase in Run OS2835 does not contradict the melting behavior described by **Reaction (1)** and **(2)**, because it seems to be a branch reaction mainly related with the jadeite that is excessive to the solubility of Na in hollandite. No evidence indicates that the occurrence of Na-CAS phase resulted in a drastic depletion of Na in hollandite, although Na-CAS phase is more stable than jadeite at high temperatures. **Figure 3.4** shows that hollandite is more refractory than Na-CAS phase. Therefore, **Reaction (1)** and **(2)** are able to summarize the melting behavior of the phase assemblage of hollandite + jadeite + stishovite at ~ 22 GPa for (K,Na)AlSi<sub>3</sub>O<sub>8</sub> compositions with Na/(K+Na) ratios up to at least 0.8. In addition, pressure seems to be a key factor to the formation of Na-CAS phase in an albitic composition at high temperatures, since Na-CAS phase occurred only at the relatively high-P condition of Run OS2835. More studies are required to clarify the melting phase relations of (K,Na)AlSi<sub>3</sub>O<sub>8</sub> under wide P-T conditions, especially for those of the end-members.

As shown in **Figure 3.1**, the Re capsules have long dimensions, implying large effects of the thermal gradient. It is suggested by the occurrence of jadeite at the coldest parts of Run OS2813 and OS2835 that these regions were under subsolidus conditions. On the other hand, two phenomena indicate that only the coldest parts with jadeite were likely under subsolidus conditions or just at the solidus conditions. One is the occurrence of Na-CAS phase at the low-T region of Run OS2835. As mentioned above, the formation of Na-CAS phase in an albitic composition is accompanied by partial melting. Therefore, the low-T phase assemblage of Run OS2835 containing Na-CAS phase should not be regarded as a subsolidus phase assemblage. As shown in **Table 3.2**, the other phenomenon is that the hollandite adjacent to the melt has the relatively low Na contents of 44-57 mol %, because of the melting, while the hollandite became enriched in Na, up to 60-75 mol % with decreasing temperature along the thermal gradient from

the high-T to low-T region in each capsule. This is contrary to the solid-solution behavior under subsolidus conditions described in **Section 2.3** that the solubility of Na in hollandite positively correlates with temperature at a constant pressure. According to **Reaction (1)** and **(2)**, hollandite becomes depleted in Na with melting proceeding (increasing temperature above the solidus), and conversely, hollandite becomes enriched in Na with condensation proceeding (decreasing temperature toward the solidus). Thus, it is suggested by the negative temperature dependence of the solubility of Na in hollandite that the hollandite at the low-T regions of the three runs is also the product of partial melting.

The “subsolidus” hollandite at the coldest parts of Run OS2813 and OS2835 contains 69 and 75 mol % Na, respectively (**Table 3.2**), close to but less than the maximal solubility of Na in hollandite obtained under subsolidus conditions, ~ 80 mol % at 22 GPa and 2273 K (see **Section 2.3**). Considering the P-T conditions of these two runs (**Table 3.1**: OS2813, 22.5 GPa and 2575 K; OS2835, 23.5 GPa and 2675 K), one may suppose that the “subsolidus” hollandite buffered by jadeite and stishovite even has Na contents lower than the just-mentioned maximal solubility obtained at a similar pressure of 22 GPa and a relatively low temperature of 2273 K, thus, the temperature differences through the capsules can be as large as 300-400 K. However, such large temperature gradients are not expected, because the low-T grains could not grow up to 10-20  $\mu\text{m}$  (**Figure 3.2b**, **3.2d** and **3.2f**) at relatively low temperatures like 2273 K within the short durations of 30 and 90 minutes (**Table 3.1**), according to the synthesis experience at 20-23 GPa and 2273 K mentioned in **Section 2.3**. A possible interpretation to the issue about the composition of hollandite can be that the actual pressures of the melting experiments are likely lower than the nominal values estimated by the pressure calibration at 1873 K, due to the high-T heating at ~ 2600 K, and the solubility of Na in hollandite significantly decreases from the maximal value with decreasing pressure from ~ 22 GPa, according to the pressure dependence of the solubility of Na in hollandite described in **Section 2.3**.

### 3.4 Subsolidus and melting experiments of $K_{0.05}Na_{0.85}Ca_{0.10}Al_{1.1}Si_{2.9}O_8$ at 22 GPa

A subsolidus experiment (Run OS2892, see **Table 2.2**) was performed at 22 GPa and 2273 K using two starting materials of  $K_{0.2}Na_{0.8}AlSi_3O_8$  and  $K_{0.05}Na_{0.85}Ca_{0.10}Al_{1.1}Si_{2.9}O_8$ . **Table 2.3** and **3.3** list compositions of the recovered products. **Figure 3.5** shows micro textures of the recovered samples. The composition of  $K_{0.2}Na_{0.8}AlSi_3O_8$  turned into a phase assemblage of  $K_{0.22}Na_{0.77}Al_{0.99}Si_{3.01}O_8$  hollandite + trace CF + trace stishovite. This result is comparable to those described in **Section 2.3**. The composition of  $K_{0.05}Na_{0.85}Ca_{0.10}Al_{1.1}Si_{2.9}O_8$  became a phase assemblage of jadeite + stishovite + hollandite + CAS phase. The hollandite contains 58 mol % Na and 16 mol % Ca, with 74 mol % K substituted by Na and Ca, similar to the  $(K_{0.22}Na_{0.77})-Al_{0.99}Si_{3.01}O_8$  hollandite obtained in the other capsule in terms of the substitution proportion of K. The CAS phase contains 66 mol % Ca, 31 mol % Na and 3 mol % K, while this Na (in fact,  $NaAl_3Si_3O_{11}$ ) content is obviously lower than the solubility of  $NaAl_3Si_3O_{11}$  component in CAS phase estimated by Akaogi et al. (2010), ~ 70 mol % at 22 GPa and 2273 K. This discrepancy is resulted from the fact that Akaogi et al. (2010) investigated the solid solutions of CAS phase in the system  $CaAl_4Si_2O_{11}-NaAl_3Si_3O_{11}$ , while the CAS phase was synthesized using an albitic composition in this study. The formation of Na-CAS phase in an albitic composition requires partial melting, as mentioned in **Section 3.3**. Similarly, Na-rich CAS phase does not form in an albitic composition under subsolidus conditions.

On the other hand, the incorporation of  $NaAl_3Si_3O_{11}$  component in the CAS phase indicates that some components rich in Na, Si and O, such as the speculated  $Na_2Si_2O_5$  shown in **Reaction (3)** and **(4)**, have been separated. However, probably due to the small amount, these components were not found. **Figure 3.5b** clearly shows that jadeite has the absolute advantage in abundance over other phases. Thus, although the Ca content of jadeite is low (**Table 3.3**), a large amount of Ca is supposed to be trapped in jadeite. As a result, the Ca-bearing CAS phase occurred just in a small amount, and so did the components rich in Na, Si and O. The separated



Na, Si and O could be absorbed by other phases, if the amounts are small. **Figure 3.5c** and the corresponding elemental mappings show that the CAS phase exists only at the area neighboring the capsule, where the temperature is slightly higher than that of the inside area. In addition, no evidence of melting was found in the capsule.

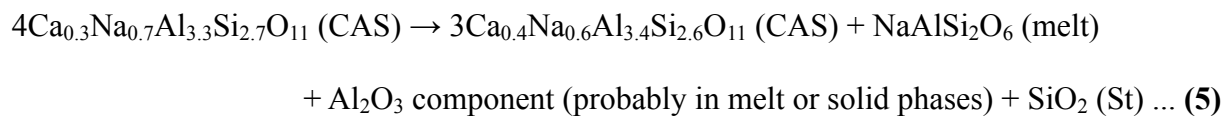
Four melting experiments were conducted at 22 GPa and 2475-2700 K with the starting composition of  $K_{0.05}Na_{0.85}Ca_{0.10}Al_{1.1}Si_{2.9}O_8$ . The experimental conditions and results are listed in **Table 3.1**. The samples are small, but the grains are large (10-20  $\mu\text{m}$ ), thus low-magnification observation plus elemental mapping exhibits both micro textures of the whole samples and the distribution of each phase, as shown in **Figure 3.6**. Each phase can be easily recognized by its characteristic element, that is, hollandite is K-bearing; jadeite or melt, Na; CAS phase, Ca and Al; stishovite, Si.

**Figure 3.6a** shows that the phase assemblage obtained at 22 GPa and 2475 K is quench crystals (at the hottest part of the capsule) + stishovite + CAS phase + hollandite + jadeite (at the coldest part), which is the same to the subsolidus phase assemblage obtained at 22 GPa and 2273 K, except for the quench crystals. Therefore, the temperature of 2475 K is supposed to be slightly higher than the solidus temperature. With increasing temperature from 2475 to 2700 K at 22 GPa, jadeite did not occur at 2500 K (**Figure 3.6b**), and hollandite was almost used up at 2600 K (**Figure 3.6c**), and only a thin layer of CAS phase survived behind a stishovite layer at 2700 K (**Figure 3.6d**); the volume fraction of melting increased from  $\sim 35\%$  at 2500 K to  $\sim 60\%$  at 2700 K. The melting sequence has shown that jadeite is the solidus phase followed by hollandite and then CAS phase, and stishovite is the liquidus phase. The textural difference between **Figure 3.6a** and **3.6b** can be hardly explained by the negligible temperature difference between Run OS2908 (2475 K) and OS2909 (2500 K). Either of the temperatures was possibly misestimated by the thermocouple. But even so, a solidus temperature of  $\sim 2400$  K is acceptable for the composition of  $K_{0.05}Na_{0.85}Ca_{0.10}Al_{1.1}Si_{2.9}O_8$  at 22 GPa.

**Table 3.3** lists compositions of the recovered products. In contrast to the phases formed at the subsolidus condition of 22 GPa and 2273 K, the phases formed at temperatures above the solidus have compositional changes as follows: the jadeite formed at 22 GPa and 2475 K has a similar composition, which is stoichiometric, and contains trace Ca and undetectable K; more Na (72 mol % versus 58 mol %) and less Ca (8 mol % versus 16 mol %) have been incorporated in the hollandite formed at 22 GPa and 2475 and 2500 K (the actual temperature difference is larger, as discussed above); the CAS phases are rich in Na, ~ 65 mol %, much higher than the Na content of 31 mol % obtained at 22 GPa and 2273 K, and have become a dominant phase in the phase assemblages of partial melting at 22 GPa and 2475-2600 K. The CAS phase survived at 22 GPa and 2700 K has a composition of  $K_{0.08}Na_{0.54}Ca_{0.40}Al_{3.35}Si_{2.63}O_{11}$ , which is depleted in Na and enriched in Ca and K, in comparison to the CAS phases formed at 22 GPa and 2475-2600 K. The stishovite obtained in the five subsolidus or melting experiments contains trace Al, and the K, Na and Ca contents in the stishovite are below the detection limit. The melt generated at 22 GPa and 2600 and 2700 K has jadeitic compositions with ~ 4 mol % K, ~ 87 mol % Na and ~ 9 mol % Ca (normalized). The melt generated at 22 GPa and 2500 K has a composition of  $K_{0.03}Na_{1.28}Ca_{0.08}Al_{0.76}Si_{2.07}O_6$ , which is obviously depleted in Al and slightly enriched in Na (92 mol %, normalized). Due to the small amounts, compositions of the melt generated at 22 GPa and 2475 K and the hollandite formed at 22 GPa and 2600 K were not measured.

It is verified by the enrichment of Na in CAS phase above the solidus temperature that the formation of Na-rich CAS phase in an albitic composition requires partial melting. The Al-depleted (Na- and Si-enriched, in other words) jadeitic melt generated at 22 GPa and 2500 K implies that the melting of jadeite partly followed the melting behavior described in **Reaction (4)**, and some components rich in Na, Si and O have been released into the melt. It can be seen from **Table 3.3** that the Na content of CAS phase slightly increased from 63 mol % at 2475 K to 68 mol % at 2600 K, although Na behaved less compatible than Ca and K. This indicates that

the melting of CAS phase did not occur at 22 GPa and 2475-2600 K. The Ca solved in the melt likely derived from jadeite and hollandite. The melting of CAS phase began in the temperature range of 2600-2700 K at 22 GPa, as indicated by the depletion of Na in CAS phase (**Table 3.3**) and the reduction of the volume fraction of CAS phase at 22 GPa and 2700 K (**Figure 3.6d**). A large amount of CAS phase was melted at 22 GPa and 2700 K, while the generated melt still kept a stoichiometrically jadeitic composition, similar to that generated at 22 GPa and 2600 K (**Table 3.3**), indicating that the partial melting of Na-rich CAS phase likely generated a jadeitic melt, similar to that of Na-rich hollandite (**Reaction (2)**). To describe the partial melting of Na-rich CAS phase at 22 GPa and 2700 K, a simplified reaction is made, as shown in **Reaction (5)**. It should be pointed out that Ca is preserved completely in **Reaction (5)**, which is unrealistic for the real melting process.



It seems that the partial melting of  $\text{K}_{0.05}\text{Na}_{0.85}\text{Ca}_{0.10}\text{Al}_{1.1}\text{Si}_{2.9}\text{O}_8$  at 22 GPa and 2475-2700 K did not consume stishovite. In fact, more stishovite was formed from the partial melting of Na-rich hollandite and CAS phase during the proceeding of melting, as revealed by **Reaction (2)** and **(5)**. The volume fraction of stishovite seems to have increased with the proceeding of melting from 2475 to 2700 K at 22 GPa, as shown in **Figure 3.6**.

The positive temperature dependence of the solubility of Na ( $\text{NaAl}_3\text{Si}_3\text{O}_{11}$  component) in CAS phase at 22 GPa and 2475-2600 K is similar to the solid-solution behavior of (Ca,Na)-CAS phase under subsolidus conditions, which was reported by Akaogi et al. (2010). At 22 GPa, the solubility of Na in CAS phase reached the maximal value of 68 mol % at 2600 K. The maximal solubility likely increases with increasing pressure to 23.5 GPa, since Na-CAS phase has been synthesized at 23.5 GPa and 2675 K (Run OS2835).

Jadeite was melted up at 22 GPa and 2500 K, while hollandite did not lose Na during the proceeding of melting from 2475 to 2500 K at 22 GPa, although Na behaved less compatible than Ca and K. The melting of jadeite indicates the beginning of partial melting, and therefore the solubility of Na in hollandite at 22 GPa reached the maximum of 72 mol % at 2500 K, since the solubility of Na in hollandite positively correlates with temperature at a constant pressure under subsolidus conditions (see **Section 2.3**). In the binary or ternary systems, all the hollandite obtained at ~ 22 GPa in the temperature range above 2273 K and below the solidus temperature has similar substitution proportions of K, 75-80 mol %, as indicated by the  $K_{0.2}Na_{0.8}AlSi_3O_8$  and  $K_{0.23}Na_{0.58}Ca_{0.16}Al_{1.11}Si_{2.89}O_8$  hollandite obtained at the subsolidus condition of 22 GPa and 2273 K (see **Section 2.3** and **3.4**) and the  $K_{0.25}Na_{0.75}Al_{0.99}Si_{3.01}O_8$  and  $(K_{0.20}Na_{0.72}Ca_{0.07}Al_{1.06})-Si_{2.94}O_8$  hollandite obtained at the solidus conditions.

### **3.5 Quench crystals obtained in the partial melting of $K_{0.2}Na_{0.8}AlSi_3O_8$**

The partial melting of  $K_{0.2}Na_{0.8}AlSi_3O_8$  was achieved at ~ 23 GPa and ~ 2600 K (**Table 3.1**), and the jadeitic melt (**Table 3.2**) has crystallized during quenching (**Figure 3.1**).

**Figure 3.2a, 3.2c, 3.2e, 3.7a** and **3.7b** show micro textures of the quench crystals found in the partial melting of  $K_{0.2}Na_{0.8}AlSi_3O_8$ . It can be seen that columnar crystals with large sizes up to 20-50  $\mu m$  almost fill up the melting regions. Compositional analyses (**Table 3.2**) show that these crystals have hollandite-like compositions with high Na/(K+Na) ratios (0.75-0.83) and abnormally high Al/(Al+Si) ratios (0.28-0.32 versus the normal value of 0.25 for (K,Na)- $AlSi_3O_8$  hollandite). Quench crystals form under extremely non-equilibrium conditions, and the diffusion of constituent is insufficient. Consequently, quench crystals have compositions which may deviate from the equilibrium composition. Rapid crystallization during quenching also led to the scattered compositions of the hollandite-like quench crystals shown in **Table 3.2**.

**Figure 3.3a** shows the XRD pattern of the quench crystals of Run OS2809, and the peaks can be interpreted by a mixture of hollandite and CF. The quench crystals of Run OS2835

were also identified by XRD, and a similar result was obtained. **Figure 3.8a** shows the Raman spectrum of the large quench crystals of Run OS2835, and the vibration modes are comparable to those of the hollandite synthesized in Run OS2741 (**Table 2.2**). The large quench crystals of Run OS2809 were also identified using Raman spectroscopy, and a similar result was obtained. The structural evidence proves that the large quench crystals obtained in the partial melting of  $K_{0.2}Na_{0.8}AlSi_3O_8$  are hollandite-structured.

Liu (2006) obtained a  $K_{0.50(4)}Na_{0.46(6)}Al_{1.30(7)}Si_{2.79(5)}O_8$  hollandite in a partial melting of  $K_{0.2}Na_{0.8}AlSi_3O_8$  at 22 GPa and 2673 K, and regarded it as a solid phase. It can be seen that the strange hollandite obtained by Liu (2006) resembles the quench crystals of hollandite obtained in this study, both texturally and compositionally. Therefore, the former is not a solid phase but a quench product.

The CF revealed by XRD has small sizes of  $\sim 3 \mu m$ , as shown in **Figure 3.7a**. The CF grains were carefully searched and then analyzed by EDS, and the compositions are CF-like, as shown in **Table 3.2**. Jadeite appeared as the solidus phase at the coldest parts of the capsules, as described in **Section 3.3**, while CF crystallized from the jadeitic melt during quenching. This likely indicates that the dissociation of jadeite into CF and stishovite has a positive Clapeyron slope, as suggested by Akaogi et al. (2002) and Kawai and Tsuchiya (2012). The pressures of  $\sim 23$  GPa used in the melting experiments of  $K_{0.2}Na_{0.8}AlSi_3O_8$  are close to the phase boundary at 1273-2273 K reported by Akaogi et al. (2010). It seems that jadeite was stabilized at the solidus temperature, while CF crystallized from the jadeitic melt, when the P-T condition of the melt entered into the stability region of CF at relatively low temperatures during quenching.

Besides the quench crystals of hollandite and CF, quench products in another type were found in the melting regions, which are named “rest” tentatively. Only compositions of the rest were analyzed by EDS, and electron-beam damages were found at the analyzed areas after the analyses. As shown in **Table 3.2**, the rest has highly Na- and Si-enriched compositions, such as

$K_{0.03}Na_{1.54}Al_{0.32}Si_{1.87}O_5$  (Run OS2835), and the contents of K and Al in the rest are quite low, in comparison to the content of K in the quench crystals of hollandite and the content of Al in the jadeitic melt, respectively. From the compositions of the jadeitic melt, the hollandite quench crystals and the rest, it is expected that large amounts of K and Al in the jadeitic melt helped to form the hollandite quench crystals with abnormally high Al/(Al+Si) ratios during quenching, and the rest was left with compositions enriched in Na and Si.

### 3.6 Quench crystals obtained in the partial melting of $K_{0.05}Na_{0.85}Ca_{0.10}Al_{1.1}Si_{2.9}O_8$

The partial melting of  $K_{0.05}Na_{0.85}Ca_{0.10}Al_{1.1}Si_{2.9}O_8$  was achieved at 22 GPa and 2475-2700 K (**Table 3.1**), and the jadeitic melt (**Table 3.3**) has crystallized during quenching (**Figure 3.6**).

**Figure 3.6** clearly shows the distributions of phases and elements in the partial melting of  $K_{0.05}Na_{0.85}Ca_{0.10}Al_{1.1}Si_{2.9}O_8$ . Micro textures of the melting regions are shown in **Figure 3.7c** and **3.7d**. It can be seen that columnar quench crystals have grain sizes of 2-10  $\mu\text{m}$ , and the rest dominates large volumes in the melting regions. The elemental mappings of **Figure 3.6** indicate that the jadeitic melt transformed into two parts during quenching, Al-bearing quench crystals and the rest highly enriched in Na. **Table 3.3** shows that the rest has highly enriched Na and Si and highly depleted K, Ca and Al, such as  $K_{0.02}Na_{1.45}Ca_{0.05}Al_{0.39}Si_{1.81}O_5$  (Run OS2909), similar to the rest found in the partial melting of  $K_{0.2}Na_{0.8}AlSi_3O_8$ .

The Al-bearing quench crystals are compositionally divided into two types, hollandite-like and CAS-like (**Table 3.3**). Due to the compositional differences, the two types of quench crystals are recognizable in the elemental mappings. As shown in **Figure 3.6b** and **3.6d**, the K-rich areas in the melting regions reflect the hollandite-like quench crystals, and the green color (representing Al) at the K-rich areas are deeper than those at the rest and lighter than those of the CAS-like quench crystals. The hollandite-like quench crystals have high Na contents, such

as  $K_{0.14}Na_{0.72}Ca_{0.10}Al_{1.15}Si_{2.87}O_8$  (Run OS3007), and the slightly high Al/(Al+Si) ratios possibly resulted from the incorporation of Ca. The CAS-like quench crystals also have high Na contents (Na/(K+Na+Ca) ratios: 0.78, Run OS2909; 0.67, Run OS2911; 0.69, Run OS3007). The CAS-like quench crystals obtained in Run OS2909 and OS3007 have respective compositions of  $K_{0.04}Na_{0.84}Ca_{0.20}Al_{2.84}Si_{3.05}O_{11}$  and  $K_{0.06}Na_{0.57}Ca_{0.20}Al_{2.46}Si_{3.40}O_{11}$ , and the Al and Si numbers of these compositions are incompatible with the molar totals of K, Na and Ca, if these CAS-like quench crystals are CAS-structured. In addition, it is also shown in **Figure 3.6b** and **3.6d** that the CAS-like quench crystals are more abundant than the hollandite-like quench crystals. **Figure 3.7c** and **3.7d** show that the hollandite-like quench crystals are 3-5 times larger than the CAS-like quench crystals.

**Figure 3.8a** shows Raman spectra of the hollandite-like quench crystals found in Run OS2909 and OS3007, and the main vibration modes are comparable to those of the hollandite synthesized in Run OS2741 (**Table 2.2**). The structural evidence proves that the hollandite-like quench crystals are hollandite-structured. Raman spectra of the CAS-like quench crystals found in Run OS2909 and OS3007 are shown in **Figure 3.8b**, and Raman spectra of the CAS phases coexisting with stishovite and the jadeitic melt are also shown as references. It is likely that the neighboring stishovite was involved in the Raman measurements conducted on the crystals of CAS phases, so that vibration modes of stishovite appear in the Raman spectra of CAS phases (**Figure 3.8b**: Run OS2909, CAS; Run OS3007, CAS). **Figure 3.8b** shows that the CAS-like quench crystals have vibration modes comparable to those of the CAS phases, and the vibration modes at  $\sim 298$ ,  $\sim 634$ ,  $\sim 868$  and  $\sim 920$   $cm^{-1}$  correspond to those of Ca-CAS phase at 280, 616, 851 and 910  $cm^{-1}$  in Beck et al. (2004) and at 290, 624, 855 and 910  $cm^{-1}$  in Zhai and Ito (2008), respectively. The differences in Raman shift are probably due to the compositional differences. Ca-CAS phase ( $CaAl_4Si_2O_{11}$ ) was analyzed in the previous studies, while the CAS phases and the CAS-like quench crystals analyzed in this study contain large amounts of Na, and also the

corresponding Al and Si numbers are quite different from those of Ca-CAS phase, because of the incorporation of Na in the CAS structure. The structural evidence proves that the CAS-like quench crystals are CAS-structured.

Vibration modes of stishovite can be seen in the Raman spectrum of the quench crystals of CAS phase found in the melting region of Run OS3007, as shown in **Figure 3.8b**. However, no compositionally stishovite-like quench crystals were found. An intergrowth of CAS phase and stishovite during quenching is suggested by the Raman spectrum showing vibration modes of both CAS phase and stishovite, and probably interprets the compositional abnormality of the quench crystals of CAS phase found in Run OS3007 (**Table 3.3**): the Si number of 3.40 is much higher than the normal values of 2 and 3 for Ca- and Na-CAS phases, respectively; the molar deviations of Al and Si (0.16 and 0.14, respectively) are 1-2 times larger than those of any other quench crystals (e.g., Run OS2909, Q CAS, Al 0.07, Si 0.05). The large molar deviations of Al and Si may suggest inhomogeneous distributions of the quench-formed stishovite among the quench crystals of CAS phase.

The quench crystals of stishovite only appeared in Run OS3007, among the seven runs performed in this study (**Table 3.1**), based on the phase identifications using XRD (mainly used in the partial melting of  $K_{0.2}Na_{0.8}AlSi_3O_8$ , because of the large sizes of the melting regions) and Raman spectroscopy. The intergrowth of quench-formed CAS phase and stishovite in Run OS-3007 is likely related to the capsule material of Re, while diamond was used as capsules in the other runs performed using the composition of  $K_{0.05}Na_{0.85}Ca_{0.10}Al_{1.1}Si_{2.9}O_8$ . The cooling rates affected by the capsule materials may have affected the formation of quench crystals. Relative to Re, diamond may have higher thermal conductivity at HPHT, so that the cooling duration (in other words, the crystallization duration during quenching) in Run OS3007 might be slightly longer than those of the other runs using diamond capsules. In comparison to Al-bearing phases like hollandite and CAS phase, stishovite may have a sluggish kinetics of crystallization, even



in the case of liquid crystallization, thus the relatively long cooling duration of Run OS3007 was necessary for the crystallization of stishovite from the jadeitic melt.

In addition, vibration modes of stishovite do not appear in the Raman spectrum of the quench-formed hollandite in Run OS3007 (**Figure 3.8a**), indicating no intergrowth of quench-formed hollandite and quench-formed stishovite. Relative to hollandite-like compositions (e.g.,  $(\text{K},\text{Na})\text{AlSi}_3\text{O}_8$ ), jadeitic compositions (e.g.,  $\text{NaAlSi}_2\text{O}_6$ ) are depleted in Si; relative to CAS-like compositions (e.g.,  $\text{NaAl}_3\text{Si}_3\text{O}_{11}$ ), jadeitic compositions are enriched in Si. This may simply interpret why stishovite crystallized from the jadeitic melt during quenching only together with CAS phase, because the formation of stishovite needs excessive Si components, which might be generated by the formation of CAS phase in the jadeitic melt during quenching.

### **3.7 Implications for the shock metamorphism of plagioclase in strongly shocked meteorites**

As described in **Chapter 2** and **3**, both Na-rich hollandite and Na-rich CAS phase can form in albitic compositions at  $\sim 22$  GPa by two ways: (1) equilibrium formation in the stability regions and (2) non-equilibrium formation as quench crystals during quenching.

For the typical albitic composition of plagioclase in meteorites,  $\text{Ab}_{85}\text{An}_{10}\text{Or}_5$ , a large amount ( $\sim 80$  mol %) of potassium in hollandite can be substituted by Na (and Ca) only within a narrow pressure range at 22 GPa above 2273 K below the solidus temperature of  $\sim 2400$  K. But even so, Na-rich hollandite is not a dominant phase in the phase assemblage of  $\text{Ab}_{85}\text{An}_{10}\text{Or}_5$  at 22 GPa and 2273-2400 K. At temperatures below 2273 K, hollandite is just a minor phase in the phase assemblage of  $\text{Ab}_{85}\text{An}_{10}\text{Or}_5$ , due to the low substitution proportions in hollandite at relatively low temperatures (e.g., Yagi et al. 1994; Ishii et al. 2012). Therefore, the subsolidus phase relations of  $\text{Ab}_{85}\text{An}_{10}\text{Or}_5$  cannot interpret the formation of lingunite in albitic plagioclase in strongly shocked meteorites, because jadeite should be more abundant. If lingunite formed

via solid-state transformation, studies such as Kubo et al. (2010, 2016) are needed to investigate the kinetic factors of the crystallization of each phase in the phase assemblages of  $\text{Ab}_{85}\text{An}_{10}\text{Or}_5$ . Partial melting of  $\text{Ab}_{85}\text{An}_{10}\text{Or}_5$  at 22 GPa also cannot be the interpretation, because previous observations did not show any evidence for partial melting. Also, CAS phase is quite dominant in the partial melting of  $\text{Ab}_{85}\text{An}_{10}\text{Or}_5$  at 22 GPa, while CAS phase has never been discovered in the shock metamorphism of albitic plagioclase in strongly shocked meteorites.

Na-rich hollandite and Na-rich CAS phase can form as quench crystals in jadeitic melt at 22 GPa, as shown in **Chapter 3**, although neither hollandite nor CAS phase is the liquidus phase in the composition of  $\text{Ab}_{85}\text{An}_{10}\text{Or}_5$  at 22 GPa. The experimental results suggest that the crystallization behavior of the jadeitic melt is mainly controlled by Al, and also K and Ca, and the energy barrier for the crystallization of aluminosilicate in the jadeitic melt seems lower than those of stishovite and jadeite (and calcium ferrite-type  $\text{NaAlSiO}_4$ ), and even K and Ca in minor amounts are decisive for the crystallization of hollandite and CAS phase, respectively. It should be pointed out that the crystallization of Na-rich hollandite and Na-rich CAS phase occurred in the partial melting of  $\text{Ab}_{85}\text{An}_{10}\text{Or}_5$ , while partial melting is not supported by the appearance of the shock metamorphism of albitic plagioclase. Based on the experimental results of this study, it can be expected that if a complete melting of  $\text{Ab}_{85}\text{An}_{10}\text{Or}_5$  occurs, the crystallization behavior of the albitic melt will not change, that Ca-bearing and Na-rich CAS phase crystallizes together with stishovite during quenching, and K-bearing and Na-rich hollandite solely crystallizes. This is because the difference between the jadeitic melt and the albitic melt is just a silica component, briefly speaking, as shown in **Table 2.1, 3.2 and 3.3**, which should not affect too much. At 22 GPa, both Na-rich hollandite and Na-rich CAS phase occur in an albitic melt during quenching. However, no CAS phase has been discovered in the shock metamorphism of albitic plagioclase. Therefore, a complete melting of  $\text{Ab}_{85}\text{An}_{10}\text{Or}_5$  and the subsequent quenching at 22 GPa may not interpret the formation of lingunite in strongly shocked meteorites, but it is still necessary to investigate the effect of pressure on the crystallization behavior of albitic melt.

Although the formation of lingunite was not interpreted by the experimental results of this study, the crystallization of Na-rich CAS phase in the partial melting of  $\text{Ab}_{85}\text{An}_{10}\text{Or}_5$  helps to understand the shock metamorphism of labradoritic plagioclase in some Martian meteorites. As mentioned in **Chapter 1**, the plagioclase in Martian meteorites has a typical composition of  $\text{Ab}_{47}\text{An}_{51}\text{Or}_2$ , and the corresponding shock metamorphism includes maskelynite, Na-rich CAS phase and stishovite (Chen and El Goresy 2000; Beck et al. 2004; El Goresy et al. 2013). Also, Ca-rich lingunite was discovered in addition to Na-rich CAS phase and stishovite.

The composition of  $\text{Ab}_{47}\text{An}_{51}\text{Or}_2$  has an  $\text{Al}/(\text{Al}+\text{Si})$  ratio of 0.3775, similar to those of the jadeitic melt shown in **Table 3.2** and **3.3**, about 0.33. The crystallization behavior of a labradoritic melt is probably similar to that of the jadeitic melt, and CAS phase and stishovite may crystallize from the labradoritic melt during quenching. This basically matches the coexistence of Na-rich CAS phase and stishovite in the Martian meteorite Zagami (Beck et al. 2004). Some experiments are needed to confirm whether the CAS phase formed in a labradoritic melt can be rich in Na. However, in the natural cases, due to the small grain sizes, it is difficult to measure compositions of the shock-metamorphic CAS phases precisely (Beck et al. 2004; El Goresy et al. 2013). The trace K in  $\text{Ab}_{47}\text{An}_{51}\text{Or}_2$  likely resulted in the occurrence of hollandite nearly the CAS phase and stishovite in the Martian meteorite Zagami (Beck et al. 2004).

In the Martian meteorite NWA856, stishovite- and CAS phase-dominated regions were observed in a large melt pool (El Goresy et al. 2013). The occurrence of stishovite-dominated region possibly derived from an active crystallization of stishovite as the liquidus phase in the labradoritic melt, which further suggests that the stishovite-dominated region had a relatively low cooling rate. Otherwise, CAS phase should crystallize together with stishovite, as shown in Run OS3007, because the crystallization of stishovite in either a jadeitic melt or a labradoritic melt will cause an increase of Al in the residual part of the melt.

Different cooling rates of the shock veins may highly affect the shock metamorphism of plagioclase. Some previous studies proposed that the occurrence of high-pressure phases in or adjacent to the shock veins is due to the high-temperature conditions. In the case of the shock metamorphism of plagioclase, a complete melting of plagioclase could be achieved at the local pressure spikes, where very high temperatures could be generated, due to the closure of porous areas (Sharp and DeCarli 2006; Beck et al. 2007). These compacted and melted areas are the so-called “melt pockets”. The melt pockets of plagioclase far away from the shock veins were rapidly quenched by the surrounding cold minerals, and then became glass (maskelynite), while the melt pockets of plagioclase in or adjacent to the shock veins were relatively slowly cooled, which insured sufficient durations for the crystallization of aluminosilicates from the melt.

The composition of  $\text{Ab}_{85}\text{An}_{10}\text{Or}_5$  was not completely melted at 22 GPa and 2700 K, suggesting that the peak temperatures of labradoritic melt pockets were probably much higher than 2700 K, if stishovite is assumed to be the liquidus phase in labradoritic compositions. As modeled by Sharp et al. (2015), a 1.6 mm shock vein with starting temperatures (in other words, peak temperatures) of 3500 and 2500 K can be solidified at  $\sim 2273$  K within  $\sim 1.9$  s and  $750 \mu\text{s}$ , respectively; the 1.6 mm shock vein can be cooled down from 3500 K to 1500 K within  $\sim 5$  s, and the temperature of 1500 K is proposed to be a lower limit for the back transformations of shock-metamorphic high-pressure phases (like ringwoodite and lingunite) under low pressures within a duration of  $\sim 4$  s. Similarly, based on the model given by Sharp et al. (2015), for small-scaled melt pockets (e.g., 10-200  $\mu\text{m}$ ), much shorter durations than  $\sim 1.9$  and  $\sim 5$  s are required to solidify the melt pockets and preserve the shock-metamorphic high-pressure phases under low pressures, respectively. In the melting experiments of this study, the melting regions of the samples have similar dimensions, relative to the melt pockets. Just after the moment that heating was stopped by cutting off the power supply, the thermocouple reflected that the temperature jumped from target temperatures like 2700 K down to 400-500 K immediately. Although it is difficult to know the cooling rates of the samples, the quenching did not last for more than 0.2-

0.3 s. Such durations are comparable to those inferred for natural shock events,  $\sim 0.01$ -1 s (e.g., Beck et al. 2005). It can be seen that the micro textures of the quench-formed CAS phase (plus stishovite) (**Figure 3.7c** and **3.7d**) are close to those observed in the Martian meteorites Zagami and NWA856 (Beck et al. 2004; El Goresy et al. 2013). The active nucleation of CAS phase in the labradoritic melt was likely due to the relatively high contents of Al and Ca, in comparison to the limited nucleation of CAS phase in albitic melt. Durations for the crystallization of CAS phase from the labradoritic melt in the Martian meteorites might be at the same magnitude as those of the melting experiments of this study.

**Figure 3.9** summarizes the experimental conditions and results listed in **Table 3.1**. The subsolidus phase assemblage of  $\text{Ab}_{85}\text{An}_{10}\text{Or}_5$  at 19-22 GPa is jadeite + stishovite + hollandite + CAS phase. The solidus temperatures of  $\text{Ab}_{85}\text{An}_{10}\text{Or}_5$  at 19 and 22 GPa are  $\sim 2400$  and  $\sim 2475$  K, respectively, close to those of KLB-1 peridotite (Zhang and Herzberg 1994), while the liquidus temperature of  $\text{Ab}_{85}\text{An}_{10}\text{Or}_5$  at 19-22 GPa seems to be at least 100 K higher than that of KLB-1 peridotite (Zhang and Herzberg 1994). Therefore, if the melting phase relations of KLB-1 peridotite are used to infer the P-T conditions of shock veins, and if oligoclase melted completely at 19-22 GPa during impact, the oligoclase could be hotter than the shock veins. On the other hand, the liquidus temperature of oligoclase at 19-22 GPa is close to those of olivine and pyroxene, 2700-2900 K. Whole-rock melting might occur above the liquidus temperatures of both chondritic and feldspathic compositions during impact, which consequently triggered the formation of shock veins and maskelynite, and the peak temperature could be high enough to melt the grains of olivine and pyroxene surrounding the shock veins, partially or completely. However, individual melting of olivine and pyroxene is relatively rare (Miyahara et al. 2009), compared with that of plagioclase. Most  $\text{MgSiO}_3$ -rich glasses discovered in shocked meteorites are suggested to be the amorphized  $\text{MgSiO}_3$ -rich perovskite named bridgmanite (Tschauner et al. 2014). It is unexpected that the shock-vein temperature selectively melted the surrounding oligoclase and ignored the surrounding olivine and pyroxene. Thus, the shock-vein temperature

may be not essential for the melting of oligoclase during impact, and a localized heating within oligoclase is expected. Such a process has been described in detail in Sharp and DeCarli (2006) and Gillet and El Goresy (2013) that due to the low shock impedance of feldspar, the refracted shock waves among minerals with different shock impedance may collide in feldspar and cause localized pressures much higher than the continuum shock pressure. After the localized pressure goes down and equilibrates the continuum shock pressure, the waste heat can lead to localized high temperatures like  $\sim 3000$  K and melt the compressed feldspar. Later, the feldspathic melt can be cooled down by heat transfer to the surrounding minerals. The cooling rate dominates the formation of quench product, maskelynite by an ultrafast cooling or crystalline phases by a cooling in  $\sim 0.1$ -1 s. To further understand the melting of feldspar and also the whole rock, the kinetics must be considered.

## Chapter 4

### New high-pressure forms of $\text{Al}_2\text{SiO}_5$

#### 4.1 Introduction

Kyanite ( $\text{Al}_2\text{SiO}_5$ ), the high-pressure polymorph of andalusite and sillimanite, is a typical metamorphic mineral in Al-rich eclogites, and also occurs in subducted continental and sedimentary materials (e.g., Irifune et al. 1994; Ono 1998; Schmidt et al. 2004). Kyanite is stable up to 12-13 GPa at 1273-1900 K, and dissociates into corundum and stishovite with further increasing pressure (e.g., Irifune et al. 1995; Ono et al. 2007).

Ahmed-Zaïd and Madon (1991, 1995) ever obtained a  $\text{V}_3\text{O}_5$ -type  $\text{Al}_2\text{SiO}_5$  in the DAC experiments performed at 40-70 GPa and  $\sim 2500$  K using natural samples of kyanite, grossular and pyrope as starting materials, and proposed it as a possible host mineral of aluminum in the lower mantle. However, this  $\text{V}_3\text{O}_5$ -type  $\text{Al}_2\text{SiO}_5$  has never been experimentally reproduced, and remains mysterious (Kesson et al. 1995; Funamori et al. 1997; Miyajima et al. 1999; Liu et al. 2016). On the other hand, Oganov and Brodholt (2000) investigated a series of  $\text{Al}_2\text{SiO}_5$  phases including the hypothetical  $\text{V}_3\text{O}_5$  type via ab initio calculation, and contradicted the  $\text{V}_3\text{O}_5$ -type  $\text{Al}_2\text{SiO}_5$  reported by Ahmed-Zaïd and Madon (1991), based on the large discrepancies in the lattice parameters and density of  $\text{V}_3\text{O}_5$ -type  $\text{Al}_2\text{SiO}_5$  between the experimental values and the calculated results.

Recently, an unknown  $\text{Al}_2\text{SiO}_5$  phase was found in a melting experiment of  $(\text{K}_{0.2}\text{Na}_{0.8})\text{-AlSi}_3\text{O}_8$  at 22.5 GPa and 2650 K, which is structurally different from andalusite, sillimanite and kyanite. This unknown  $\text{Al}_2\text{SiO}_5$  phase was subsequently reproduced by multi-anvil experiments, and its structure was studied by X-ray and electron diffraction. Meanwhile, phase relations of  $\text{Al}_2\text{SiO}_5$  were investigated at 13-23 GPa and 2200-2800 K.

## 4.2 Experimental methods

### 4.2.1 Starting materials

Two kinds of starting materials were used: (1) synthetic kyanite and (2) oxide mixtures of quartz and corundum. The kyanite was synthesized at 7 GPa and 1673 K using an 18/11 cell assembly with a graphite tubular heater. The starting materials were stored at 383 K and sealed in Re capsules before HPHT experiments. No attention was paid to avoid the starting materials being moistened by water in air during sample loading, and no hydrous phase was found in the recovered samples. The trace water in the starting materials may have helped the grain growth of the products.

### 4.2.2 HPHT experiments

The multi-anvil high-pressure apparatuses mentioned in **Section 2.2.2** were used for HPHT experiments. The modified 10/4 cell assembly mentioned in **Section 3.2.2** was used, and MgO and LaCrO<sub>3</sub> were used as electrical and thermal insulators surrounding Re capsule and Mo electrodes, respectively. **Figure 2.1d** shows the schematic diagram of the 10/4 cell assembly.

The HPHT experiments were made at 13-23 GPa and 2200-2800 K. **Table 4.1** lists the experimental conditions and results. Due to the lack of pressure markers available for HPHT quench-recovery experiments at 2200-2800 K, the pressure calibration at 1873 K (**Figure 2.2**) was used to estimate the pressures at 2200-2800 K. A W<sub>97</sub>Re<sub>3</sub>-W<sub>75</sub>Re<sub>25</sub> thermocouple was used to monitor the temperature, and no correction was made for the effect of pressure on the electromotive force of the thermocouple. In a few runs, the thermocouples broke during compression or reported abnormal temperature values during heating, then the temperatures were estimated based on the repeatable power-temperature relationships.



### 4.2.3 Analytical methods

Structural, morphological and compositional analyses using XRD, FESEM and EDS, respectively, are basically the same as those mentioned in **Section 2.2.3**. **Figure 4.1** shows XRD patterns of some typical samples.

For electron microscopic observation and compositional analysis, the polished samples were coated with carbon. Back-scattered electron images of some typical samples are shown in **Figure 4.2**. Quartz and corundum were used as the standards for Si and Al, respectively. **Table 4.2** and **4.3** list compositions of the recovered products.

For structural identification using electron diffraction, thin films were cut out from the top surface of the samples using a focused ion beam (FIB) system (FEI<sup>TM</sup> Scios). Selected area electron diffraction (SAED) was performed within a transmission electron microscope (TEM, JEOL JEM-2100F).

### 4.3 Structural identification of unknown Al<sub>2</sub>SiO<sub>5</sub> phases

The unknown Al<sub>2</sub>SiO<sub>5</sub> phase found in the melting experiment of K<sub>0.2</sub>Na<sub>0.8</sub>AlSi<sub>3</sub>O<sub>8</sub> (see **Section 3.3**) was successfully reproduced using the same composition at 17-23 GPa and 2500-2800 K, as supported by the XRD patterns shown in **Figure 3.3b** and **4.3a**. The peaks at 20.49°, 21.46°, 28.82° and 33.03° are characteristic for this unknown Al<sub>2</sub>SiO<sub>5</sub> phase.

Using the crystallographic parameters of the hypothetical V<sub>3</sub>O<sub>5</sub>-type Al<sub>2</sub>SiO<sub>5</sub> reported by Oganov and Brodholt (2000), the XRD pattern of the unknown Al<sub>2</sub>SiO<sub>5</sub> phase was basically identified, as shown in **Figure 4.3a**, and preliminary lattice parameters were calculated. Then, plenty of SAED patterns of the unknown Al<sub>2</sub>SiO<sub>5</sub> phase (some are shown in **Figure 4.5a**) were interpreted with attempts. It was clarified by Åsbrink (1980) and Hong and Åsbrink (1982) that the structure of V<sub>3</sub>O<sub>5</sub> has two modifications with space groups of P2/c (No. 13) or C2/c (No. 15). Oganov and Brodholt (2000) considered that remarkable pairs of face-sharing octahedra

tend to be occupied by Al rather than Si to reduce the cation-cation electrostatic repulsion, and then chose C2/c for V<sub>3</sub>O<sub>5</sub>-type Al<sub>2</sub>SiO<sub>5</sub>. When interpreting the SAED patterns, it was found that d values of the diffraction spots matched the d values calculated using C2/c, while C2/c could not satisfy the SAED patterns. By testing other monoclinic space groups, it was found that C2 (No. 5), Cm (No. 8) and C2/m (No. 12) could interpret the SAED patterns, revealing the diffraction rule that the present hkl spots must have  $h + k = 2n$  (n is an integer), as shown in **Figure 4.5a**.

Oganov and Brodholt (2000) reported three configurations of lattice parameters for the hypothetical V<sub>3</sub>O<sub>5</sub>-type Al<sub>2</sub>SiO<sub>5</sub>. Following the diffraction rule that  $h + k = 2n$  (n is an integer) for hkl diffraction, the three configurations yield the same diffraction patterns (both XRD and SAED), and the only difference is in the hkl index. Since the crystallographic parameters of the unknown Al<sub>2</sub>SiO<sub>5</sub> phase, including the space group and the lattice parameters, were determined preliminarily, based on those reported by Oganov and Brodholt (2000), it is definitely suggested that the unknown Al<sub>2</sub>SiO<sub>5</sub> phase synthesized at 17-23 GPa and 2500-2800 K possesses a V<sub>3</sub>O<sub>5</sub>-type structure. However, at this stage, it is difficult to find out the appropriate lattice parameters, because a key SAED pattern needs to be taken along the b axis. Also, more work is required to further determine the space group of V<sub>3</sub>O<sub>5</sub>-type Al<sub>2</sub>SiO<sub>5</sub>.

The space group of C2/m and the “Cell choice 2” (a configuration of lattice parameters given by Oganov and Brodholt (2000)) were tentatively chosen for V<sub>3</sub>O<sub>5</sub>-type Al<sub>2</sub>SiO<sub>5</sub>, and the lattice parameters were calculated using 15 XRD peaks in a two-theta range of 15-75 degree. **Table 4.4** list the observed and the calculated d values. **Table 4.5** list lattice parameters of V<sub>3</sub>O<sub>5</sub>-type Al<sub>2</sub>SiO<sub>5</sub>. The lattice parameters are  $a = 9.2964 \text{ \AA}$ ,  $b = 4.7068 \text{ \AA}$ ,  $c = 6.6272 \text{ \AA}$  and  $\beta = 111.30^\circ$ . If 4 is chosen as the Z number, V<sub>3</sub>O<sub>5</sub>-type Al<sub>2</sub>SiO<sub>5</sub> is 1.3 % less dense than the isochemical mixture of corundum and stishovite. The lattice parameters and the (relative) density of V<sub>3</sub>O<sub>5</sub>-type Al<sub>2</sub>SiO<sub>5</sub> in this study agree with the theoretically calculated results of Oganov and Brodholt (2000), and contradict those reported by Ahmed-Zaid and Madon (1991).

At 14-17 GPa and 2550-2750 K, another unknown  $\text{Al}_2\text{SiO}_5$  phase was found. **Figure 4.3b** shows the corresponding XRD patterns. It was found that this  $\text{Al}_2\text{SiO}_5$  phase structurally differs from andalusite, sillimanite, kyanite and  $\text{V}_3\text{O}_5$ -type  $\text{Al}_2\text{SiO}_5$ . To make a clear definition, it is tentatively named “ $\delta$ - $\text{Al}_2\text{SiO}_5$ ”, if andalusite, sillimanite, kyanite are regarded as  $\alpha$ -,  $\beta$ - and  $\gamma$ - $\text{Al}_2\text{SiO}_5$ , respectively. Similarly,  $\text{V}_3\text{O}_5$ -type  $\text{Al}_2\text{SiO}_5$  is  $\epsilon$ - $\text{Al}_2\text{SiO}_5$ . Using the software Dicvol 04 (Boultif and Louër 2004), the XRD pattern of  $\delta$ - $\text{Al}_2\text{SiO}_5$  (**Figure 4.3b**) can be indexed to a triclinic cell with lattice parameters  $a = 6.7695(35) \text{ \AA}$ ,  $b = 10.9624(25) \text{ \AA}$ ,  $c = 10.5225(45) \text{ \AA}$ ,  $\alpha = 125.392(35)^\circ$ ,  $\beta = 138.549(35)^\circ$  and  $\gamma = 58.733(30)^\circ$ . The unit cell volume of  $\delta$ - $\text{Al}_2\text{SiO}_5$  is  $416.15 \text{ \AA}^3$ , and the density is  $3.880 \text{ g/cm}^3$ , if the unit cell contains six formula units ( $Z = 6$ ). The present XRD pattern indexing of  $\delta$ - $\text{Al}_2\text{SiO}_5$  satisfies its SAED patterns (**Figure 4.5b**), and the latter shows no specific diffraction rules, indicating that the space group is likely P1 (No. 1) or P-1 (No. 2).

XRD patterns of the  $\delta$ - $\text{Al}_2\text{SiO}_5$  obtained in Run OS2986, OS2988 and OS2991 are somehow different from each other (**Figure 4.4**), especially in the peak intensity. The  $\delta$ - $\text{Al}_2\text{SiO}_5$  synthesized at 14-17 GPa and 2550-2750 K has large grain sizes of 50-100  $\mu\text{m}$ , as shown in **Figure 4.2e**, so that the grains of  $\delta$ - $\text{Al}_2\text{SiO}_5$  are highly oriented, which resulted in the fact that among the XRD patterns shown in **Figure 4.4**, the relative peak intensity is variable, and not all the peaks in one pattern appear in the other patterns. It can be seen from **Table 4.6** that most of the  $d$  values are repeatable, indicating that the samples have the same structure. The  $d$  values of  $\text{V}_3\text{O}_5$ -type  $\text{Al}_2\text{SiO}_5$  reported by Ahmed-Zaid and Madon (1991) are also listed in **Table 4.6** for comparison. Although some of their data are similar to those of this study, it is difficult to infer that their  $\text{V}_3\text{O}_5$ -type  $\text{Al}_2\text{SiO}_5$  is likely the  $\delta$ - $\text{Al}_2\text{SiO}_5$  obtained in this study, because much less diffraction was observed in their study, even with X-ray powder diffraction.

#### 4.4 Phase relations of $\text{Al}_2\text{SiO}_5$ at 13-23 GPa and 2200-2800 K

**Figure 4.2** shows micro textures of some typical samples. Run OS3006 yielded a fine-grained mixture of kyanite, corundum and stishovite at 14.2 GPa and 2200 K (**Figure 4.1a** and **4.2a**), indicating that the phase boundary of kyanite dissociation extends to higher pressures and temperatures than those studied previously (Irfune et al. 1995; Ono et al. 2007). In Run OS3004, the starting material of kyanite was completely melted at 13 GPa and 2675 K, and the recovered quench crystals are shown in **Figure 4.2b**. It is strange that the bulk composition of the quench crystals deviate from  $\text{Al}_2\text{SiO}_5$  (**Table 4.3**:  $\text{Al}_{1.72}\text{Si}_{1.21}\text{O}_5$ ), which implies a partial melting of the starting material. However, the observed sample shows a complete melting, and no additional Al component was found. Since this melted sample was not contaminated, it is still regarded as a useful sample.  $\text{V}_3\text{O}_5$ -type  $\text{Al}_2\text{SiO}_5$  was synthesized at 17-23 GPa and 2500-2800 K. It was found that when using the starting material of oxide mixtures, the obtained  $\text{V}_3\text{O}_5$ -type  $\text{Al}_2\text{SiO}_5$  contains residual corundum and stishovite, especially those obtained at relatively low-temperature conditions, as shown in **Figure 4.1c** and **4.2c**; when using the starting material of kyanite, the recovered samples show no coexistence of two different phase assemblages: the synthesized  $\text{V}_3\text{O}_5$ -type  $\text{Al}_2\text{SiO}_5$  is pure, as shown in **Figure 4.1d** and **4.2d**, and the recovered mixture of corundum and stishovite contains no  $\text{V}_3\text{O}_5$ -type  $\text{Al}_2\text{SiO}_5$ , as shown in **Figure 4.1b**. In the case of the synthesis using the starting material of oxide mixtures, the initial chemical inhomogeneity was difficult to eliminate within limited durations even at high temperatures, due to the sluggish kinetics, and the Al- and Si-bearing components, in forms of corundum and stishovite, respectively, could survive at different sides of the reaction band, as shown in **Figure 4.2c**. Because of the high-temperature heating, the samples of  $\delta\text{-Al}_2\text{SiO}_5$  synthesized at 15-16 GPa and 2550-2750 K have large grain sizes of 50-100  $\mu\text{m}$ , as shown in **Figure 4.2e**.

**Figure 4.6** shows phase relations of  $\text{Al}_2\text{SiO}_5$  at 13-23 GPa and 2200-2800 K. Based on the experimental results, preliminary phase boundaries have been drawn. At 13 GPa, kyanite

is stable up to 2400 K, and the solidus temperature at 13 GPa is  $\sim 2500$  K. The phase boundary of kyanite dissociation has a positive Clapeyron slope (e.g., Irifune et al. 1995; Ono et al. 2007). In this study, kyanite dissociated into a mixture of corundum and stishovite at 14.2 GPa and 2200 K. This agrees with the experimental results of Irifune et al. (1995) and Ono et al. (2007), and the difference in pressure is  $\sim 1$  GPa between the result of this study and the extrapolated phase boundaries of the two previous studies. The mixture of corundum and stishovite are stable at the low-temperature side at 14-23 GPa, while the newly discovered  $\delta$ -Al<sub>2</sub>SiO<sub>5</sub> and V<sub>3</sub>O<sub>5</sub>-type Al<sub>2</sub>SiO<sub>5</sub> dominate the high-temperature side at 14-17 and 17-23 GPa, respectively. It seems that the phase boundary between V<sub>3</sub>O<sub>5</sub>-type Al<sub>2</sub>SiO<sub>5</sub> and the mixture of corundum and stishovite has a positive Clapeyron slope, and the transition pressure is described as  $P$  (GPa) =  $0.03T$  (K) – 55.75. The phase boundary between  $\delta$ -Al<sub>2</sub>SiO<sub>5</sub> and the mixture of corundum and stishovite also likely has a positive Clapeyron slope. The triple point of  $\delta$ -Al<sub>2</sub>SiO<sub>5</sub>, V<sub>3</sub>O<sub>5</sub>-type Al<sub>2</sub>SiO<sub>5</sub> and the mixture of corundum and stishovite is located at 16.5 GPa and 2400 K, and the triple point of  $\delta$ -Al<sub>2</sub>SiO<sub>5</sub>, kyanite and the mixture of corundum and stishovite is located at 14 GPa and 2250 K. The phase boundaries drawn in **Figure 4.6** are preliminarily determined, and more systematic experiments using low-pressure cell assemblies are needed to further constrain the phase boundaries.

**Table 4.2** shows that both the obtained  $\delta$ -Al<sub>2</sub>SiO<sub>5</sub> and V<sub>3</sub>O<sub>5</sub>-type Al<sub>2</sub>SiO<sub>5</sub> have ideally stoichiometric compositions of Al<sub>2</sub>SiO<sub>5</sub>. Due to the small grain sizes, most of the stishovite in the mixture of corundum and stishovite was not analyzed by EDS. Due to the high-temperature heating, the stishovite within V<sub>3</sub>O<sub>5</sub>-type Al<sub>2</sub>SiO<sub>5</sub> has relatively large grain sizes (e.g., **Figure 4.2c**), and the compositions were measured by EDS. **Table 4.3** shows that the stishovite within V<sub>3</sub>O<sub>5</sub>-type Al<sub>2</sub>SiO<sub>5</sub> (except Run OS2954) contains trace Al (< 2 wt %). As shown in **Table 4.1**, the starting material of Run OS2868 is Si-rich (Al<sub>2</sub>Si<sub>1.5</sub>O<sub>6</sub>) relative to Al<sub>2</sub>SiO<sub>5</sub>, and the product is a mixture of V<sub>3</sub>O<sub>5</sub>-type Al<sub>2</sub>SiO<sub>5</sub> and stishovite. Run OS2868 indicates that there are no other

phases with compositions between  $\text{Al}_2\text{SiO}_5$  and  $\text{SiO}_2$  within the stability region of  $\text{V}_3\text{O}_5$ -type  $\text{Al}_2\text{SiO}_5$ . It was found that corundum grew faster than stishovite at the same condition, as shown in **Figure 4.2a** and **4.2c**. Some corundum formed with stishovite at relatively low-temperature conditions has grain sizes available for compositional analysis. **Table 4.3** shows that corundum coexisting with stishovite,  $\delta\text{-Al}_2\text{SiO}_5$  or  $\text{V}_3\text{O}_5$ -type  $\text{Al}_2\text{SiO}_5$  could contain 10-15 wt %  $\text{SiO}_2$  at 15-23 GPa and 2375-2550 K. Systematic studies are needed to investigate the effects of pressure and temperature on the solubility of  $\text{SiO}_2$  in corundum.

Run OS2852 was performed with the composition of  $\text{Al}_2\text{Si}_{1.5}\text{O}_6$  at 21.3 GPa and 2800 K, and a phase assemblage including  $\text{V}_3\text{O}_5$ -type  $\text{Al}_2\text{SiO}_5$ , stishovite and an unknown  $\text{Al}_2\text{Si}_2\text{O}_7$  phase was obtained after the HPHT experiment (**Table 4.1**). **Figure 4.7** shows the micro texture and elemental mappings of the recovered sample. **Table 4.2** shows compositions of the  $\text{V}_3\text{O}_5$ -type  $\text{Al}_2\text{SiO}_5$  and the  $\text{Al}_2\text{Si}_2\text{O}_7$  phase. Ahmed-Zaïd and Madon (1991) and Schmidt et al. (1997) also found  $\text{Al}_2\text{Si}_2\text{O}_7$  phases in their experiments, but only few details were reported. Schmidt et al. (1997) proposed that kyanite dissociated into the  $\text{Al}_2\text{Si}_2\text{O}_7$  phase and corundum at 18 GPa and  $\sim 2773$  K. The formation condition of the  $\text{Al}_2\text{Si}_2\text{O}_7$  phase in this study is comparable to that reported by Schmidt et al. (1997). Due to the excessive  $\text{SiO}_2$  component in the starting material, corundum did not occur in Run OS2852, because the corundum generated by the dissociation of  $\text{Al}_2\text{SiO}_5$  has been used up by reacting with the excessive  $\text{SiO}_2$  component.  $\text{V}_3\text{O}_5$ -type  $\text{Al}_2\text{SiO}_5$  coexisted with the  $\text{Al}_2\text{Si}_2\text{O}_7$  phase in Run OS2852, indicating that the P-T condition was located at the phase boundary between  $\text{V}_3\text{O}_5$ -type  $\text{Al}_2\text{SiO}_5$  and the mixture of the  $\text{Al}_2\text{Si}_2\text{O}_7$  phase and corundum. The latter phase assemblage is likely stable at high-temperature conditions beyond the stability region of  $\text{V}_3\text{O}_5$ -type  $\text{Al}_2\text{SiO}_5$ .

As shown in **Figure 4.6**, quite different from Irifune et al. (1995) and Ono et al. (2007), Schmidt et al. (1997) and Liu et al. (2006) reported that the phase boundary of the dissociation of kyanite has a moderate Clapeyron slope, and kyanite is stable at 16-17 GPa and  $\sim 2300$  K.

The large discrepancy was considered to be resulted from experimental uncertainties, such as the low precision of pressure calibration (Schmidt et al. 1997; Ono et al. 2007) and the effect of water (Liu et al. 2006). However, it can be clearly seen that the pressure difference is as large as 3-4 GPa at ~ 2300 K, comparing the phase boundaries of Schmidt et al. (1997) and Liu et al. (2006) with the extrapolated phase boundaries of Irifune et al. (1995) and Ono et al. (2007). Such large discrepancy can be hardly interpreted by experimental uncertainties. In this study, kyanite dissociated into corundum and stishovite at 14.2 GPa and 2200 K, and the experiments produced mixtures of corundum and stishovite at 14-17 GPa and 2000-2375 K. These results agree with the phase boundaries of Irifune et al. (1995) and Ono et al. (2007), and are in conflict with the results of Schmidt et al. (1997) and Liu et al. (2006).

To understand the large discrepancy mentioned above, it is necessary to check the two previous studies, Schmidt et al. (1997) and Liu et al. (2006), in detail. Schmidt et al. (1997) made misleading descriptions about the phase identification of the recovered samples. It is quite unclear whether all the recovered samples were analyzed using XRD, or some of them were analyzed only by electron microprobe analysis; two experiments (1k-20 and 1k-8) at 14.5 GPa and 1273 K and 14.5 GPa and 1573 K, respectively, were directly prepared for XRD, whether phase assemblages of the other samples were identified via an indirect way, such as electron microprobe analysis or identification based on color and hardness. Schmidt et al. (1997) should have provided the XRD patterns and the electron microscopic images of the recovered samples, otherwise it is quite difficult to understand the phase transitions observed in their study, because a mixture of synthetic stishovite,  $\text{Al}_2\text{O}_3$  (likely corundum) and natural kyanite was used as the starting material, which might have some effects on the phase transitions and the micro textures. Another possibility is that the kyanite obtained by Schmidt et al. (1997) at ~ 16 GPa and ~ 2300 K was actually the newly discovered  $\delta\text{-Al}_2\text{SiO}_5$  or  $\text{V}_3\text{O}_5$ -type  $\text{Al}_2\text{SiO}_5$ , but was misrecognized as kyanite only based on electron microprobe analysis. It can be seen from **Figure 4.6** that the

temperature of  $\sim 2300$  K is  $\sim 100$  K lower than the transition temperature of  $\sim 2400$  K at 16-17 GPa. Schmidt et al. (1997) mentioned that the nominal temperatures given by thermocouples were measured at the coldest parts of the capsules, and the temperature gradients were  $\sim 100$  K over the capsule length. Therefore, the actual temperatures of their experiments can be close to 2400 K, similar to the transition temperatures estimated in this study at 16-17 GPa. Schmidt et al. (1997) obtained kyanite at  $\sim 14$  GPa and 1273-1573 K, which is not so different from Irifune et al. (1995) and Ono et al. (2007), and the pressure difference is  $\sim 2$  GPa, still can be explained by experimental uncertainties. However, Schmidt et al. (1997) probably obtained  $\delta$ -Al<sub>2</sub>SiO<sub>5</sub> or V<sub>3</sub>O<sub>5</sub>-type Al<sub>2</sub>SiO<sub>5</sub> at 16-17 GPa and  $\sim 2400$  K, thus their moderate Clapeyron slope is likely a mistake made by misrecognizing  $\delta$ -Al<sub>2</sub>SiO<sub>5</sub> or V<sub>3</sub>O<sub>5</sub>-type Al<sub>2</sub>SiO<sub>5</sub> as kyanite.

Liu et al. (2006) also did not provide clear evidence to prove the acquisition of kyanite in their experiments. It was claimed that kyanite could not be detected by X-ray, due to the very low proportion. Liu et al. (2006) showed a back-scattered electron image of a sample containing kyanite. It can be seen from the image of Liu et al. (2006) that the phase assemblage is almost corundum plus stishovite, and the grain of kyanite is quite small,  $\sim 2$   $\mu\text{m}$  in diameter. Such small grain size could be hardly available for precise compositional analysis. Also, it is quite difficult to distinguish kyanite from corundum and stishovite, based on the compositional contrast in the back-scattered electron image. Liu et al. (2006) analyzed only 3-4 grains of kyanite in each of the kyanite-containing samples, which is likely due to the low proportion. If the kyanite in their samples was rare and small, and could not be detected using XRD, it is quite difficult to believe the occurrence of kyanite in their experiments. Liu et al. (2006) probably obtained mixtures of corundum and stishovite only, thus their data could not be used to determine the phase boundary of kyanite dissociation.

It is difficult to make a direct comparison between Ahmed-Zaid and Madon (1991) and this study, since the pressures are quite different. However, their DAC experiments might have



large uncertainties in both pressure and temperature. As mentioned by Ahmed-Zaid and Madon (1995), the temperature uncertainty could be as large as 800 K, and the pressure was measured by an indirect way of using calibrated strain gauges attached to the steel body of the cell. They reported  $V_3O_5$ -type  $Al_2SiO_5$  and the  $Al_2Si_2O_7$  phase, but the structural information of their new phases is different from those of this study. It is still unclear what kinds of products they found.

Garnet and bridgmanite are, respectively, the host minerals of Al in the pyrolitic upper and lower mantle (e.g., Irifune and Ringwood 1987; Irifune 1994; Liu et al. 2016). In MORB compositions, clinopyroxene and garnet possess most of Al under the upper mantle conditions (e.g., Irifune and Ringwood 1993); under the lower mantle conditions, in addition to aluminous bridgmanite, NAL phase (e.g., Sanehira et al. 2006) and/or CF phase (Yamada et al. 1983) occur as Al-bearing phase(s) from the garnet-perovskite transformation at 23-27 GPa (e.g., Oguri et al. 2000), and can be stable up to 50 GPa (Perrillat et al. 2006) and 120 GPa (Hirose et al. 2005), respectively. The stability region of  $V_3O_5$ -type  $Al_2SiO_5$  is located at the high-temperature side beyond the geotherm. On the other hand, Oganov and Brodholt (2000) suggested that the  $V_3O_5$ -type phases does not satisfy Pauling's second rule (sum of the electrostatic bond valences on the anion should be equal to the anion's valence), so that the structure of  $V_3O_5$ -type  $Al_2SiO_5$  made by Al and Si octahedra must undergo distortions, which may destabilize the structure; in contrast, aluminosilicates with large and electropositive cations, such as  $KAlSi_3O_8$  hollandite, can be more stable. Therefore,  $V_3O_5$ -type  $Al_2SiO_5$  is unlikely a host mineral of Al in the mantle. Considering the severe stability region of  $V_3O_5$ -type  $Al_2SiO_5$ , it may form from a low-pressure polymorph of  $Al_2SiO_5$  during a strong impact.

## References

- [1] Agee CB, Li J, Shannon MC, Circone S (1995) Pressure-temperature phase diagram for the Allende meteorite. *J Geophys Res* 100: 17725-17740
- [2] Ahmed-Zaid I, Madon M (1991) A high-pressure form of  $\text{Al}_2\text{SiO}_5$  as a possible host of aluminum in the lower mantle. *Nature* 353: 426-428
- [3] Ahmed-Zaid I, Madon M (1995) Electron microscopy of high-pressure phases synthesized from natural garnets in a diamond anvil cell: implications for the mineralogy of the lower mantle. *Earth Planet Sci Lett* 129: 233-247
- [4] Akaogi M, Tanaka A, Kobayashi M, Fukushima N, Suzuki T (2002) High-pressure transformations in  $\text{NaAlSiO}_4$  and thermodynamic properties of jadeite, nepheline, and calcium ferrite-type phase. *Phys Earth Planet Inter* 130: 49-58
- [5] Akaogi M, Ajiro H, Kojitani H (2005) High-pressure phase relations of hollandite in the system  $\text{KAlSi}_3\text{O}_8$ - $\text{NaAlSi}_3\text{O}_8$ . 2005 Annual Meeting of the Mineralogical Society of Japan, Session ID K1-03
- [6] Akaogi M, Haraguchi M, Nakanishi K, Ajiro H, Kojitani H (2010) High-pressure phase relations in the system  $\text{CaAl}_4\text{Si}_2\text{O}_{11}$ - $\text{NaAl}_3\text{Si}_3\text{O}_{11}$  with implications for Na-rich CAS phase in shocked Martian meteorites. *Earth Planet Sci Lett* 289: 503-508
- [7] Åsbrink S (1980) The crystal structure of and valency distribution in the low-temperature modification of  $\text{V}_3\text{O}_5$ . The decisive importance of a few very weak reflexions in a crystal-structure determination. *Acta Cryst B* 36: 1332-1339
- [8] Beck P, Gillet P, Gautron L, Daniel I, El Goresy A (2004) A new natural high-pressure (Na,Ca)-hexalumino-silicate [ $(\text{Ca}_x\text{Na}_{1-x})\text{Al}_{3+x}\text{Si}_{3-x}\text{O}_{11}$ ] in shocked Martian meteorites. *Earth Planet Sci Lett* 219: 1-12
- [9] Beck P, Gillet P, El Goresy A, Mostefaoui S (2005) Timescales of shock processes in chondritic and Martian meteorites. *Nature* 435: 1071-1074
- [10] Beck P, Ferroir T, Gillet P (2007) Shock-induced compaction, melting and entrapment of atmospheric gases in Martian meteorites. *Geophys Res Lett* 34: L01203
- [11] Birch AF and LeComte P (1960) Temperature-pressure plane for albite composition. *Am J Sci* 258: 209-217
- [12] Boffa Ballaran T, Liu J, Dubrovinsky LS, Caracas R, Crichton W (2009) High-pressure ferroelastic phase transition in aluminosilicate hollandite. *Phys Rev B* 80: 214104
- [13] Caracas R, Boffa Ballaran T (2010) Elasticity of (K,Na) $\text{AlSi}_3\text{O}_8$  hollandite from lattice dynamics calculations. *Phys Earth Planet Inter* 181: 21-26
- [14] Chen M, Sharp TG, El Goresy A, et al. (1996) The majorite-pyrope + magnesiowüstite assemblage: constraints on the history of shock veins in chondrites. *Science* 271: 1570-1573
- [15] Chen M, El Goresy A (2000) The nature of maskelynite in shocked meteorites: not diaplectic glass but a glass quenched from shock-induced dense melt at high pressures. *Earth Planet Sci Lett* 179: 489-502
- [16] Chen M, Xie X, El Goresy A (2004a) A shock-produced (Mg,Fe) $\text{SiO}_3$  glass in the Suizhou meteorite. *Meteorit Planet Sci* 39: 1797-1808
- [17] Chen M, El Goresy A, Gillet P (2004b) Ringwoodite lamellae in olivine: clues to olivine-ringwoodite phase transition mechanisms in shocked meteorites and subducting slabs. *PNAS* 101, 15033-15037

- [18] El Goresy A, Gillet P, Miyahara M, et al. (2013) Shock-induced deformation of Shergottites: shock-pressures and perturbations of magmatic ages on Mars. *Geochimica et Cosmochimica Acta* 101: 233-262
- [19] Fei Y, Orman JV, Li J, et al. (2004) Experimentally determined postspinel transformation boundary in  $\text{Mg}_2\text{SiO}_4$  using MgO as an internal pressure standard and its geophysical implications. *J Geophys Res* 109: B02305
- [20] Ferroir T, Onozawa T, Yagi T, et al. (2006) Equation of state and phase transition in  $\text{KAlSi}_3\text{O}_8$  hollandite at high pressure. *Am Mineral* 91: 327-332
- [21] Funamori N, Yagi T, Miyajima N, Fujino K (1997) Transformation in garnet from orthorhombic perovskite to  $\text{LiNbO}_3$  phase on release of pressure. *Science* 275: 513-515
- [22] Gautron L, Angel RJ, Miletich R (1999) Structural characterization of the high-pressure phase  $\text{CaAl}_4\text{Si}_2\text{O}_{11}$ . *Phys Chem Miner* 27: 47-51
- [23] Gillet P, Chen M, Dubrovinsky L, El Goresy A (2000) Natural  $\text{NaAlSi}_3\text{O}_8$ -hollandite in the shocked Sixiangkou meteorite. *Science* 287: 1633-1636
- [24] Gillet P, El Goresy A (2013) Shock events in the solar system: the message from minerals in terrestrial planets and asteroids. *Annu Rev Earth Planet Sci* 41: 257-85
- [25] Hirao N, Ohtani E, Kondo T, Sakai T, Kikegawa T (2008) Hollandite II phase in  $\text{KAlSi}_3\text{O}_8$  as a potential host mineral of potassium in the Earth's lower mantle. *Phys Earth Planet Inter* 166: 97-104
- [26] Hirose K, Takafuji N, Sata N, Ohishi Y (2005) Phase transition and density of subducted MORB crust in the lower mantle. *Earth Planet Sci Lett* 237: 239-251
- [27] Hong SH, Åsbrink S (1982) The structure of the high-temperature modification of  $\text{V}_3\text{O}_5$  at 458 K. *Acta Cryst B* 38: 713-719
- [28] Irifune T, Ringwood AE (1987) Phase transformations in primitive MORB and pyrolite compositions to 25 GPa and some geophysical implications. *High Pressure Research in Mineral Physics: A Volume in Honor of Syun-iti Akimoto* (Eds, Manghnani MH, Syono Y), AGU, 231-242
- [29] Irifune T, Ringwood AE (1993) Phase transformations in subducted oceanic crust and buoyancy relationships at depths of 600-800 km in the mantle. *Earth Planet Sci Lett* 117: 101-110
- [30] Irifune T (1994) Absence of an aluminous phase in the upper part of the Earth's lower mantle. *Nature* 370: 131-133
- [31] Irifune T, Ringwood AE, Hibberson WO (1994) Subduction of continental crust and terrigenous and pelagic sediments: an experimental study. *Earth Planet Sci Lett* 126: 351-368
- [32] Irifune T, Kuroda K, Minagawa, Unemoto M (1995) Experimental study of the decomposition of kyanite at high pressure and high temperature. *The Earth's Central Part: Its Structure and Dynamics*, edited by Yukutake T, 35-44
- [33] Ishii T, Kojitani H, Akaogi M (2012) High-pressure phase transitions and subduction behavior of continental crust at pressure-temperature conditions up to the upper part of the lower mantle. *Earth Planet Sci Lett* 357-358: 31-41
- [34] Katsura T, Ito E (1989) The system  $\text{Mg}_2\text{SiO}_4$ - $\text{Fe}_2\text{SiO}_4$  at high pressures and high temperatures: precise determination of stabilities of olivine, modified spinel, and spinel. *J Geophys Res* 94: 15663-15670

- [35] Kawai K, Tsuchiya T (2012) High-P,T phase relations in the NaAlSi<sub>2</sub>O<sub>6</sub> system from first principles computation. *Phys Chem Miner* 39: 305-310
- [36] Kawai K, Tsuchiya T (2013) First-principles study on the high-pressure phase transition and elasticity of KAlSi<sub>3</sub>O<sub>8</sub> hollandite. *Am Mineral* 98: 207-218
- [37] Kerschhofer L, Sharp TG, Rubie DC (1996) Intracrystalline transformation of olivine to wadsleyite and ringwoodite under subduction zone conditions. *Science* 274: 79-81
- [38] Kerschhofer L, Rubie DC, Sharp TG, McConnell JDC, Dupas-Bruzek C (2000) Kinetics of intracrystalline olivine-ringwoodite transformation. *Phys Earth Planet Inter* 121: 59-76
- [39] Kesson SE, Fitz Gerald JD, Shelley JMG, Withers RL (1995) Phase relations, structure and crystal chemistry of some aluminous silicate perovskites. *Earth Planet Sci Lett* 134: 187-201
- [40] Kimura M, Suzuki A, Kondo T, et al. (2000) Natural occurrence of high-pressure phases jadeite, hollandite, wadsleyite, and majorite-pyrope garnet in an H chondrite, Yamato 75100. *Meteorit Planet Sci* 35: A87-88
- [41] Kimura M, Chen M, Yoshida Y, et al. (2003) Back-transformation of high-pressure phases in a shock melt vein of an H-chondrite during atmospheric passage: implications for the survival of high-pressure phases after decompression. *Earth Planet Sci Lett* 217: 141-150
- [42] Kirfel A, Eichhorn K (1990) Accurate structure analysis with synchrotron radiation. The electron density in Al<sub>2</sub>O<sub>3</sub> and Cu<sub>2</sub>O. *Acta Cryst A* 46: 271-284
- [43] Kubo T, Kimura M, Kato T, et al. (2010) Plagioclase breakdown as an indicator for shock conditions of meteorites. *Nat Geosci* 3: 41-45
- [44] Kubo T, Kono M, Imamura M, et al. (2016) Constraints on P-T-t conditions for the formation of metastable lingunite from plagioclase. The 57th High Pressure Conference of Japan, Abstract No. 3C11
- [45] Langenhorst F, Poirier JP (2000) 'Eclogitic' minerals in a shocked basaltic meteorite. *Earth Planet Sci Lett* 176: 259-265
- [46] Liu J, Boffa-Ballaran T, Dubrovinsky L, Frost D (2005) High pressure study of K-Na hollandite solid solution. AGU Fall Meeting 2005, Abstract No. MR31A-0125
- [47] Liu LG (1978) High-pressure phase transformations of albite, jadeite and nepheline. *Earth Planet Sci Lett* 37: 438-444
- [48] Liu X (2006) Phase relations in the system KAlSi<sub>3</sub>O<sub>8</sub>-NaAlSi<sub>3</sub>O<sub>8</sub> at high pressure-high temperature conditions and their implication for the petrogenesis of lingunite. *Earth Planet Sci Lett* 246: 317-325
- [49] Liu X, Nishiyama N, Sanehira T, et al. (2006) Decomposition of kyanite and solubility of Al<sub>2</sub>O<sub>3</sub> in stishovite at high pressure and high temperature conditions. *Phys Chem Miner* 33: 711-721
- [50] Liu X, Ohfuji H, Nishiyama N, et al. (2012) High-P behavior of anorthite composition and some phase relations of the CaO-Al<sub>2</sub>O<sub>3</sub>-SiO<sub>2</sub> system to the lower mantle of the Earth, and their geophysical implications. *J Geophys Res* 117: B09205
- [51] Liu Z, Irifune T, Nishi M, Tange Y, Arimoto T, Shinmei T (2016) Phase relations in the system MgSiO<sub>3</sub>-Al<sub>2</sub>O<sub>3</sub> up to 52 GPa and 2000 K. *Phys Earth Planet Inter* 257: 18-27
- [52] Ma C, Tschauer O, Beckett JR, Rossman GR (2015) Liebermannite: a new potassic hollandite (KAlSi<sub>3</sub>O<sub>8</sub>) from the Zagami basaltic shergottite. 46th Lunar and Planetary Science Conference

- [53] Miyajima N, Fujino K, Funamori N, Kondo T, Yagi T (1999) Garnet-perovskite transformation under conditions of the Earth's lower mantle: an analytical transmission electron microscopy study. *Phys Earth Planet Inter* 116: 117-131
- [54] Miyahara M, El Goresy A, Ohtani E, et al. (2009) Fractional crystallization of olivine melt inclusion in shock-induced chondritic melt vein. *Phys Earth Planet Inter* 177: 116-121
- [55] Miyahara M, Ozawa S, Ohtani E, et al. (2013a) Jadeite formation in shocked ordinary chondrites. *Earth Planet Sci Lett* 373: 102-108
- [56] Miyahara M, Kaneko S, Ohtani E, et al. (2013b) Discovery of seifertite in a shocked lunar meteorite. *Nat Commun* 4: 1737
- [57] Mori H (1994) Shock-induced phase transformation of the Earth and planetary materials. *Mineral J (Japanese)* 23: 171-178
- [58] Morishima H, Kato T, Suto M, et al. (1994) The phase boundary between  $\alpha$ - and  $\beta$ -Mg<sub>2</sub>SiO<sub>4</sub> determined by in situ X-ray observation. *Science* 26: 1202-1203
- [59] Nishiyama N, Rapp RP, Irifune T, et al. (2005) Stability and P-V-T equation of state of KAlSi<sub>3</sub>O<sub>8</sub> hollandite determined by in situ X-ray observations and implications for dynamics of subducted continental crust material. *Phys Chem Miner* 32: 627-637
- [60] Oganov AR, Brodholt JP (2000) High-pressure phases in the Al<sub>2</sub>SiO<sub>5</sub> system and the problem of aluminous phase in the Earth's lower mantle: ab initio calculations. *Phys Chem Miner* 27: 430-439
- [61] Oguri K, Funamori N, Uchida T, et al. (2000) Post-garnet transition in a natural pyrope: a multi-anvil study based on in situ X-ray diffraction and transmission electron microscopy. *Phys Earth Planet Inter* 122: 175-186
- [62] Ohfuji H, Yamamoto M (2015) EDS quantification of light elements using osmium surface coating. *J Mineral Petrol Sci* 110: 189-195
- [63] Ohtani E, Kimura Y, Kimura M, et al. (2004) Formation of high-pressure minerals in shocked L6 chondrite Yamato 791384: constraints on shock conditions and parent body size. *Earth Planet Sci Lett* 227: 505-515
- [64] Ono S (1998) Stability limits of hydrous minerals in sediment and mid-ocean ridge basalt compositions: implications for water transport in subduction zones. *J Geophys Res* 103: 18253-18267
- [65] Ono S, Nakajima Y, Funakoshi K (2007) In situ observation of the decomposition of kyanite at high pressures and high temperatures. *Am Mineral* 92: 1624-1629
- [66] Ozawa S, Ohtani E, Miyahara M, et al. (2009) Transformation textures, mechanisms of formation of high-pressure minerals in shock melt veins of L6 chondrites, and pressure-temperature conditions of the shock events. *Meteorit Planet Sci* 44: 1771-1786
- [67] Perrillat JP, Ricolleau A, Daniel I, et al. (2006) Phase transformations of subducted basaltic crust in the uppermost lower mantle. *Phys Earth Planet Inter* 157: 139-149
- [68] Presnall DC (1995) Phase diagrams of Earth-forming minerals. *Mineral Physics and Crystallography: A Handbook of Physical Constants* (Eds, Ahrens TJ), AGU, 248-268
- [69] Ringwood AE, Reid AF, Wadsley AD (1967) High-pressure KAlSi<sub>3</sub>O<sub>8</sub>, an aluminosilicate with sixfold coordination. *Acta Cryst* 23: 1903-1905

- [70] Sanehira T, Irifune T, Shinmei T, et al. (2006) In situ X-ray diffraction study of an aluminous phase in MORB under lower mantle conditions. *Phys Chem Miner* 33: 28-34
- [71] Sawamoto H (1987) Phase diagram of  $\text{MgSiO}_3$  at pressures up to 24 GPa and temperatures up to 2200 °C: phase stability and properties of tetragonal garnet. *High Pressure Research in Mineral Physics: A Volume in Honor of Syun-iti Akimoto* (Eds, Manghnani MH, Syono Y), AGU, 209-219
- [72] Schmidt MW, Poli S, Comodi P, Zanazzi PF (1997) High-pressure behavior of kyanite: decomposition of kyanite into stishovite and corundum. *Am Mineral* 82: 460-466
- [73] Schmidt MW, Vielzeuf D, Auzanneau E (2004) Melting and dissolution of subducting crust at high pressures: the key role of white mica. *Earth Planet Sci Lett* 228: 65-84
- [74] Schmitt RT (2000) Shock experiments with the H6 chondrite Kernouvé: pressure calibration of microscopic shock effects. *Meteorit Planet Sci* 35: 545-560
- [75] Sharp TG, DeCarli PS (2006) Shock effects in meteorites. *Meteorites and the Early Solar System II* (Eds, Lauretta, McSween HY), The University of Arizona Press, 653-677
- [76] Sharp TG, Xie Z, DeCarli PS, Hu J (2015) A large shock vein in L chondrite Roosevelt County 106: evidence for a long-duration shock pulse on the L chondrite parent body. *Meteorit Planet Sci* 50: 1941-1953
- [77] Stöffler D, Keil K, Scott ERD (1991) Shock metamorphism of ordinary chondrites. *Geochim Cosmochim Acta* 55: 3845-3867
- [78] Sueda Y, Irifune T, Nishiyama N, et al. (2004) A new high-pressure form of  $\text{KAlSi}_3\text{O}_8$  under lower mantle conditions. *Geophys Res Lett* 31: L23612
- [79] Suzuki A, Ohtani E, Morishima H, et al. (2000) In situ determination of the phase boundary between wadsleyite and ringwoodite in  $\text{Mg}_2\text{SiO}_4$ . *Geophys Res Lett* 27: 803-806
- [80] Tomioka N, Mori H, Fujino K (2000) Shock-induced transition of  $\text{NaAlSi}_3\text{O}_8$  feldspar into a hollandite structure in a L6 chondrite. *Geophys Res Lett* 27: 3997-4000
- [81] Tschauer O, Ma C, Beckett JR, et al. (2014) Discovery of bridgmanite, the most abundant mineral in Earth, in a shocked meteorite. *Science* 346: 1100-1102
- [82] Tutti F (2007) Formation of end-member  $\text{NaAlSi}_3\text{O}_8$  hollandite-type structure (lingunite) in diamond anvil cell. *Phys Earth Planet Inter* 161: 143-149
- [83] Urakawa S, Kondo T, Igawa N, Shimomura O, Ohno H (1994) Synchrotron radiation study on the high-pressure and high-temperature phase relations of  $\text{KAlSi}_3\text{O}_8$ . *Phys Chem Miner* 21:387-391
- [84] Wang W, Takahashi E (1999) Subsolidus and melting experiments of a K-rich basaltic composition to 27 GPa: implication for the behavior of potassium in the mantle. *Am Mineral* 84: 357-361
- [85] Xie X, Chen M, Wang D (2001) Shock-related mineralogical features and P-T history of the Suizhou L6 chondrite. *Eur J Mineral* 13: 1177-1190
- [86] Xie Z, Sharp TG (2004) High-pressure phases in shock-induced melt veins of the Umbarger L6 chondrite: constraints of shock pressure. *Meteorit Planet Sci* 39: 2043-2054
- [87] Xie Z, Sharp TG, DeCarli PS (2006) High-pressure phases in a shock-induced melt vein of the Tenham L6 chondrite: constraints on shock pressure and duration. *Geochim Cosmochim Acta* 70: 504-515
- [88] Xie Z, Sharp TG (2007) Host rock solid-state transformation in a shock-induced melt vein of Tenham L6 chondrite. *Earth Planet Sci Lett* 254: 433-445

- [89] Yagi A, Suzuki T, Akaogi M (1994) High pressure transitions in the system  $\text{KAlSi}_3\text{O}_8$ - $\text{NaAlSi}_3\text{O}_8$ . *Phys Chem Miner* 21: 12-17
- [90] Yamada H, Matsui Y, Ito E (1983) Crystal-chemical characterization of  $\text{NaAlSiO}_4$  with the  $\text{CaFe}_2\text{O}_4$  structure. *Mineral Mag* 47: 177-181
- [91] Yamada H, Matsui Y, Ito E (1984) Crystal-chemical characterization of  $\text{KAlSi}_3\text{O}_8$  with the hollandite structure. *Mineral J* 12: 29-34
- [92] Yamanaka T, Fukuda T, Tsuchiya J (2002) Bonding character of  $\text{SiO}_2$  stishovite under high pressures up to 30 GPa. *Phys Chem Miner* 29: 633-641
- [93] Zhai S, Ito E (2008) Phase relations of  $\text{CaAl}_4\text{Si}_2\text{O}_{11}$  at high-pressure and high-temperature with implications for subducted continental crust into the deep mantle. *Phys Earth Planet Inter* 167: 161-167
- [94] Zhang J, Herzberg C (1994) Melting experiments on anhydrous peridotite KLB-1 from 5.0 to 22.5 GPa. *J Geophys Res* 99: 17729-17742